Modeling Study of Mesospheric Planetary Waves: Genesis and Characteristics

H. G. Mayr, J. G. Mengel, E. L. Talaat, H. S. Porter, K. L. Chan
[1]Goddard Space Flight Center, Greenbelt, MD, 20771
[2]Science Systems & Applications, Inc., Lanham, MD
[3]Applied Physic Laboratory, Johns Hopkins University, Laurel, MD
[4]Furman University, Greenville, SC
[5]Hong Kong University of Science and Technology, Hong Kong, China

Summary: In preparation for the measurements from the TIMED mission and coordinated ground based observations, we discuss results for the planetary waves (PWs) that appear in our Numerical Spectral Model (NSM). The present model accounts for a tropospheric heat source in the zonal mean (m = 0), which reproduces qualitatively the observed zonal jets near the tropopause and the accompanying reversal in the latitudinal temperature variations. We discuss the PWs that are solely generated internally, i.e., without the explicit excitation sources related to tropospheric convection or topography. Our analysis shows that PWs are not produced when the zonally averaged heat source into the atmosphere is artificially suppressed, and that the PWs generally are significantly weaker when the tropospheric source is not applied. Instabilities associated with the zonal mean temperature, pressure and wind fields, which still need to be explored, are exciting PWs that have amplitudes in the mesosphere comparable to those observed. Three classes of PWs are generated in the NSM. (1) Rossby waves, (2) Rossby gravity waves propagating westward at low latitudes, and (3) Eastward propagating equatorial Kelvin waves. A survey of the PWs reveals that the largest wind amplitudes tend to occur below 80 km in the winter hemisphere, but above that altitude they occur in the summer hemisphere where the amplitudes can approach 50 m/s.

W. Hoegy

Modeling Study of Mesospheric Planetary Waves: Genesis and Characteristics

H. G. Mayr, J. G. Mengel, E. L. Talaat, H. S. Porter, K. L. Chan
[1]Goddard Space Flight Center, Greenbelt, MD, 20771
[2]Science Systems & Applications, Inc., Lanham, MD
[3]Applied Physic Laboratory, Johns Hopkins University, Laurel, MD
[4]Furman University, Greenville, SC
[5]Hong Kong University of Science and Technology, Hong Kong, China

Paper Submitted for Publication
In
Journal of Atmospheric and Solar Terrestrial Physics
October 2003

Abstract: In preparation for the measurements from the TIMED mission and coordinated ground based observations, we discuss results for the planetary waves (PWs) that appear in our Numerical Spectral Model (NSM). The NSM extends from the ground into the thermosphere and incorporates Hines' Doppler Spread Parameterization for small-scale gravity waves (GWs). The present model accounts for a tropospheric heat source in the zonal mean (m = 0), which reproduces qualitatively the observed zonal jets near the tropopause and the accompanying reversal in the latitudinal temperature variations. We discuss the PWs that are solely generated internally, i.e., without the explicit excitation sources related to tropospheric convection or topography. Our analysis shows that PWs are not produced when the zonally averaged heat source into the atmosphere is artificially suppressed, and that the PWs generally are significantly weaker when the tropospheric source is not applied. Instabilities associated with the zonal mean temperature, pressure and wind fields, which still need to be explored, are exciting PWs that have amplitudes in the mesosphere comparable to those observed. Three classes of PWs are generated in the NSM. (1) Rossby waves, which slowly propagate westward in the moving medium, are carried by the zonal winds to produce respectively eastward and westward propagating PWs (relative to the ground) in the winter and summer hemispheres below 80 km. Depending on the zonal wave number and magnitudes of the zonal winds, and under the influence of the equatorial oscillations, the PWs typically have periods between 2 and 20 days. Their horizontal wind amplitudes can exceed 40 m/s in the lower mesosphere. (2) Rossby gravity waves propagate westward at low latitudes, having periods around 2 days for zonal wave numbers m = 2 to 4. (3) Eastward propagating equatorial Kelvin waves are generated in the upper mesosphere with periods between 2 and 3 days for m = 1 and 2. A survey of the PWs reveals that the largest wind amplitudes tend to occur below 80 km in the winter hemisphere, but above that altitude they occur in the summer hemisphere where the amplitudes can approach 50 m/s. It is shown that the non-migrating tides in the mesosphere, generated by non-linear coupling between migrating tides and PWs, are significantly larger for the model with the tropospheric heat source.

I. Introduction

As is true for the troposphere and stratosphere, planetary waves (PW) feature prominently in the observed phenomenology of the mesosphere. At altitudes between 80 and 100 km, planetary wave oscillations have been observed with spacecraft measurements (e.g., Hays et al., 1993; Shepherd et al., 1993; Wu et al., 1993; Smith, 1996; 1997; Fritts et al., 1999; Wang et al., 2000)

and with ground-based observations (e.g., Muller and Nelson, 1978; Fraser et al., 1993; Craig and Elford, 1981; Burks and Leovy, 1986; Tsuda et al., 1988; Phillips, 1989; Poole, 1990; Clark et al., 1994; Fritts and Isler, 1994; Meek et al., 1996; Deng et al., 1997; Williams et al., 1999; Harris, 1994; Harris and Vincent, 1993)).

The theoretical properties of PWs in general are well understood and have been extensively discussed in the literature (e.g., Volland, 1988; Forbes, 1995). Our understanding, however, is less developed when we ask how, where, and under what dynamical conditions the waves are generated.

In the troposphere and near the ground, topographic forcing and tropical convection can generate PWs, such as the equatorially trapped Kelvin waves and Rossby gravity waves that are involved in driving the Quasi-biennial Oscillation (QBO) and Semi-annual Oscillation (SAO) in the stratosphere (Lindzen and Holton, 1968). The PWs originating in the troposphere, however, cannot propagate through the stratosphere without being partially absorbed. A significant portion of the waves observed in the mesosphere thus is likely excited in-situ, and the dynamical conditions there are well suited for that. Due to gravity wave breaking (Lindzen, 1981), the zonal circulation in the upper mesosphere reverses, and associated with that the latitudinal temperature and pressure gradients have opposite signs. The region thus becomes baroclinically unstable, which can provide the energy to excite PWs as Plumb (1983) and Pfister (1985) had proposed.

The dynamical conditions around the tropopause are to some extend similar to those in the upper mesosphere. Cumulus heating and the resulting temperature variations generate in geostrophic balance the observed zonal jets near the tropopause. The associated meridional circulation, with upwelling at the equator, produces dynamical cooling, and this causes the variation in the temperature to reverse above the zonal jets such that it increases away from the equator towards higher latitudes. In this region of the atmosphere around the tropopause, instabilities then can develop that launch PWs.

Another important aspect of this tropospheric heat source is associated with the meridional circulation it generates. As Dunkerton (1985, 1997) pointed out, the related upward vertical winds can be comparable in magnitude to the downward propagation velocity of the QBO. This affects the period of the QBO, and the dynamical forcing required to generate the oscillation then needs to be larger (Gray and Pile, 1989; Dunkerton, 1985; Kinnersley and Pawson, 1996).

Motivated by the dynamical conditions just outlined, we extended the NSM to incorporate a tropospheric heat source in the zonal mean (m = 0) to reproduce qualitatively the observed zonal jets near the tropopause and the associated variations in temperature.

After a description of the NSM, we present numerical results for the zonal mean (m = 0) that characterize (a) the global-scale seasonal variations of the zonal circulation and temperature variations, and (b) the wave driven equatorial oscillations (QBO and SAO). In the main body of the paper, we then discuss under different dynamical conditions the planetary waves and related non-migrating tides that are generated in the model. We apply spectral analysis to identify the different planetary wave modes, and conclude by summarizing the results.

II. Numerical Spectral Model (NSM)

The design of the Numerical Spectral Model (NSM) was introduced by Chan et al. (1994), and we applied 2D and 3D versions of this model to study some aspects of the middle atmosphere dynamics (Mengel et al., 1994; Mayr et al., 1997, 2001a, b). The model has been discussed in the literature and is briefly reviewed here for completeness.

The NSM is non-linear and time dependent. Formulated with spherical harmonics, the NSM delineates the dynamical components in terms of zonal wave numbers: m = 0 for the zonal mean that includes the Semiannual Oscillation (SAO) and Quasi-biennial Oscillation (QBO), and m = 1 to 4 for the tides and planetary waves. The Navier Stokes equations are solved to describe the variations around the global mean of temperature and density, covering the atmosphere from the ground up to 400 km (240 km in the present application to speed up computation). By marching in time, the equations are solved for the spherical harmonics, and their synthesis provides the solution. The non-linear terms are evaluated in physical space. The NSM is run with a vertical step size of about 0.5 km (below 120 km) and a time step of about 5 minutes.

The following external sources drive the NSM:

(1) For the zonal mean (m = 0), the heat source is due to UV radiation in the mesosphere and stratosphere taken from Strobel (1978) and due to EUV radiation in the thermosphere.

(2) For the solar driven migrating tides, the heating rates in the middle atmosphere and troposphere are taken from Forbes and Garrett (1978).

(3) Our approach in modeling the tropopause jets and associated meridional circulation, with rising motions at the equator that extend into the lower stratosphere, is partially based on the analysis and understanding developed in a series of papers (Held and Hou, 1980; Lindzen and Hou, 1988; Plumb and Hou, 1992). For simplicity, the heat source is taken to be symmetric

around the equator and independent of season. For the purpose of this study, we chose the heating rates in the troposphere such that the model qualitatively reproduces the observed features of the zonal circulation and temperature variations.

The radiative loss in the model is described in terms of Newtonian cooling, which was originally taken from Wehrbein and Leovy (1982). More recently, we have applied in our model the cooling parameterization of Zhu (1989).

The NSM incorporates the Doppler Spread Parameterization (DSP) for small-scale gravity waves (GW), formulated by Hines (1997a, b). The theory for this parameterization was developed in a series of earlier papers (Hines, 1991a, b), and it has recently been further solidified (Hines, 2001, 2002). The DSP deals with a spectrum of waves that interact with each other to produce Doppler spreading. This affects the interaction of the waves with the background flow, which is important for the dynamics of the middle atmosphere in general and for generating the QBO in particular. The DSP has been applied also successfully in a number of other models (e.g., Akmaev, 2001; Manzini et al., 1997).

In the NSM, the GW source at the initial height (for the present model taken to be 7.5 km) is assumed to be isotropic and independent of latitude and season. The DSP assures conservation of GW momentum (and energy), and this requires at each altitude, latitude and longitude that a system of nonlinear equations be solved involving GW parameters, background winds, and buoyancy frequency. The equations are solved with Newtonian iteration, and convergence is assured by adjusting the time integration step. With an adjustable parameterization factor, the DSP also provides height dependent eddy diffusion rates (isotropic), which are incorporated into the NSM under the assumption that the variations with latitude and season can be ignored for simplicity. The heating rates associated with the dissipation of GWs are not accounted for.

III. Zonal Mean (m = 0)

In Figure 1 we present for December solstice contour plots of (a) the temperature perturbations (around the global mean) and (b) the zonal winds, both computed with the tropospheric heat source. In the troposphere up to 10 km, the applied heat source causes the temperature to increase at low latitudes around the equator and to decrease at mid to high latitudes. Above the tropopause, in the lower stratosphere, the temperature decreases around the equator and increases towards higher latitudes, which is in qualitative agreement with observations. The pressure variations associate with these temperature variations produce in

geostrophic balance zonal jets near the tropopause, which have velocities close to 15 m/s that are somewhat smaller than those observed.

In the stratosphere and lower mesosphere, the computed temperatures decrease in winter and increase in summer due to the seasonal variations of solar heating. Higher up in the mesosphere, however, the latitudinal temperature gradient reverses as a result of gravity wave interaction with the zonal circulation (Lindzen, 1981), which produces the anomalous low temperatures in the summer hemisphere that are observed. Commensurate with the temperature variations, the zonal winds in the stratosphere are eastward in winter and westward in summer below 80 km, but they reverse in the upper mesosphere.

As pointed out earlier, the configurations of the computed wind and temperature fields in the mesosphere (Figures 1a and 1b) imply that the latitudinal gradients of pressure and temperature have opposite signs, and this is conducive to generate the baroclinic instability that has been invoked to generate planetary waves (Plumb, 1983). With the temperature reversal near the tropopause, the dynamical conditions there are similar, which would explain the planetary waves, later discussed, that are being generated there.

The other aspect of the tropospheric heat source relates to the upwelling at low latitudes, which is associated with the meridional circulation that in turn causes the above discussed temperature reversal above the tropopause. The vertical winds presently generated in the model near the equator are on average about 0.15 mm/s at 30 km, which are smaller than the values inferred from water vapor anomalies (Mote et al., 1996). Vertical winds even of this magnitude can affect significantly the QBO, which is reproduced in Figure 3. The apparent amplitude of the QBO is relatively small in the present model, but the period is about 28 months close to the middle of the observed range. Without the tropospheric source (and vanishing vertical winds below 20 km), the zonal wind oscillations (not shown) have periods that are much shorter, only about 18 months. Considering the uncertainties in the adopted parameters, the model is not unique. We could have produced a QBO without the tropospheric source by choosing lower eddy diffusion rates or by releasing the GWs at lower altitudes for example. And we could also have generated larger QBO amplitudes with a larger GW source that is well within the parameter constraints of the DSP.

For the purpose of this paper, no attempt was made to tune the model to reproduce the observations. We are attempting here primarily to show what kind of PWs the NSM can produce under different conditions and in particular under the influence of the tropospheric source.

IV. Planetary Wave Genesis

Anticipating the numerical results to be discussed, we show with Figure 3 a schematic, which illustrates the dynamical features and processes that are involved in generating the PWs in the NSM. For the modeling study presented here, we emphasize that no explicit PW source of any kind is prescribed, neither thermal nor through momentum forcing. The model is driven by solar heating, which is the source for (a) the mean zonal circulation and (b) the westward migrating diurnal and semi-diurnal tides. In addition, a steady source of parameterized small-scale gravity waves (GW) is imposed, which for simplicity is taken to be independent of latitude and season. As outlined in Figure 3 and earlier discussed, the GWs produce temperature and wind reversals in the upper mesosphere (1). They also affect significantly the tides (2) and planetary waves (3). It was demonstrated for the NSM (Mayr et al., 2003) that non-linear coupling between migrating tides and PWs can produce non-migrating tides in the upper mesosphere with amplitudes comparable to those observed. By artificially turning off the solar heating for the mean zonal circulation, the PWs were suppressed in the model and so were the non-migrating tides. As Figure 3 illustrates, the GWs contribute in several important ways to the non-migrating tides by influencing significantly their building blocks, i.e., the tides and PWs. Without GWs, the mean zonal circulation would be significantly different, which in turn can affect the instabilities that generate the PWs. The GWs also contribute to the non-linear coupling (5) between the tides and PWs. And the GWs generate the QBO and amplify the SAO (4).

To elucidate some of the sources of PWs and the regions where they originate in the NSM, we present numerical results obtained under three different conditions. Generated by the full source that drives the zonal-mean ($m = 0$) circulation, including the above discussed tropospheric heating, we show for zonal wave numbers $m = 1$ to 4 the zonal winds in Figure 4a and the temperature perturbations in Figure 4b, both computed at 48° latitude and 90 km altitude. These PW oscillations are highly variable but reveal persistent seasonal variations as seen for example in the short period waves during summer months for $m = 3$ and 4 and in the long period waves around equinox that appear in all the wave numbers. For comparison, we present in Figure 5a the PWs for the zonal winds computed from a model without the tropospheric heat source. In this case, the short period PWs for $m = 3$ and 4 in summer are comparable to those in Figure 4a, but otherwise the PW amplitudes are significantly smaller. Finally, we show in Figure 5b the PWs computed without the $m = 0$ source throughout the atmosphere, and the amplitudes then are

negligibly small (note the differences in the scales). This indicates that the PWs are generated by instabilities, as illustrated in Figure 3, which still need to be identified.

It is appropriate here to show some results for the non-migrating tides, which are generated by non-linear coupling (Figure 3) involving PWs. Two solutions are presented in Figures 6a and 6b for the m = 0 non-migrating diurnal tide and in Figures 6c and 6d for the m = 1 semi-diurnal tide, computed in each case with and without the influence from the tropospheric m = 0 heat source. (One can readily verify that these tides are generated with the m = 1 PWs.) Without the tropospheric source (b, d), the computed amplitudes are significant, and they reveal systematic seasonal variations. But with the source, the amplitudes are much larger commensurate with the differences in the PWs shown in Figures 4a and 5a.

Prominent PWs are generated in the model for m = 3 (and 4, not presented) at low latitudes, which have periods between 2 and 4 days, and we show the meridional winds and temperature variations in Figures 7a and 7b respectively for a number of altitudes from 20 to 90 km. These are Rossby gravity waves, and Plumb (1983) proposed that they are generated during solstice by the instabilities that develop in the latitudinal variations (across the equator) of the zonal mean (m = 0) state variables. The 2-day waves dominate in the winds and temperature, except at 20 km where the long period waves prevail with relatively small amplitudes.

Close examination of the PWs for m = 3 (and 4, not presented) reveals that the seasonal variations drastically change when we go from the upper stratosphere into the mesosphere. This is shown with Figures 8a and 8b, where we present respectively at 60 and 90 km contour plots for the m = 3 meridional winds. To bring out the patterns, we suppressed the contour levels below 50% of the wind maxima, which are quoted in the figure headings (i.e., 27 m/s in each case). At 60 km, the largest PWs are generated preferentially in the winter hemisphere, and the waves extend across the equator into the summer hemisphere. At 90 km, the PWs also extend across the equator, but the waves appear mainly in the summer hemisphere.

V. Planetary Wave Modes

In the limited space of a paper it is not possible to provide a comprehensive description of the PWs that are generated. We therefore restrict ourselves to present a few samples that appear to be representative.

When we examine the propagation velocities of the waves at mid latitudes, we find that they are closely related to the background zonal winds. The waves apparently originate as Rossby waves that slowly propagate westward (e.g., Volland, 1988). As the waves propagate upward,

they are carried by the mean zonal circulation and get Doppler shifted to propagate eastward in winter and westward in summer.

To reveal the properties of these waves, and those of other wave modes, we present here the results from a spectral analysis of the PWs. For a limited time span after solstice (24 to 26 model months), a Fourier analysis is performed to determine the wave periods. Running windows are applied that are multiples (factor of 3 in the present case) of a given period, and the largest amplitudes are recorded.

In Figures 9a, and 9b, we present for m = 3 and at 60 km, as functions of latitude, the amplitudes of the zonal and meridional winds respectively, having periods between 1 and 10 days. For this altitude, in the winter and summer hemispheres at mid to high latitudes, the waves propagate eastward (solid lines) and westward (dashed) respectively. We consider the wave period $\tau = \lambda/U$, where U is the background zonal wind and $\lambda = 2\pi r * \cos(\theta)/m$, with r the Earth radius and θ the latitude. From this we expect that the PW periods are shorter at mid to high latitudes than those closer to the equator, as Figure 9b shows in particular for the winter hemisphere. To account for the convergence in the flow field, we note that in Rossby waves the meridional winds increase in magnitude with latitude relative to the zonal winds (Volland, 1988). The amplitudes for the meridional winds of the westward propagating Rossby gravity waves (earlier discussed) peak near the equator, and the periods are around 3 days. Consistent with that, the zonal winds for these waves tend to straddle the equator (Figure 9a).

At 90 km altitude for comparison, the spectra (Figure 9c, and 9d) are different in that the eastward propagating PWs no longer show up. The westward propagating PWs completely dominate to convey a picture in which the Rossby gravity waves around the equator appear to have merged with the westward propagating Rossby waves that originate at lower altitudes in the summer hemisphere. With Figure 10, we then present a composite picture of the altitude variations for the m = 3 PWs with periods between 2 and 4 days. Consistent with Figure 9, the larger wave amplitudes appear near 60 km in the winter hemisphere, but near 90 km in the summer hemisphere. Around the equator, the Rossby gravity waves prevail throughout the region at least between 50 and 100 km. At mid latitudes around 65 km altitude, the Rossby waves dominate that are carried by the mean zonal winds (relative to the ground) eastward in winter and westward in summer.

The PWs for m = 1 are of particular interest, because their periods are rather long, and they provide a good geometric match for interaction with the migrating tides to generate some of the largest non-migrating tides in the NSM. Analogous to Figures 9a and 9b, we show in Figures

11a and 11b the spectra for the m = 1 waves at 60 km, which differ in that they do not vanish at the poles unlike those for m > 1. (The Mercator projection is applied to expand the region at high latitudes where the waves are prominent.) The PWs at 60 km have periods around 5 days in the winter hemisphere and they propagate eastward, while those in the polar summer hemisphere have periods around 8 days and propagate westward. The increase in the oscillation period relative to m = 3 and the directions of propagation in both hemispheres are consistent with the earlier portrayed picture of Rossby waves that are carried (and Doppler shifted) by the zonal wind field. Going to 100 km (Figure 11c, and 11d), the spectra for these PWs reveal to some extent the trend seen in m = 3 (Figure 9). The eastward propagating PWs are no longer prominent, and the periods for the westward propagating waves in the summer hemisphere are shortened. Eastward propagating Kelvin waves now appear in the zonal winds at low latitudes (Figure 11c), which have periods between 2 and 4 days.

In Figure 12, we present the altitude variations of the zonal and meridional winds for the m = 1 PWs with periods from 2 to 4 days (a, b) and from 4 to 10 days (c, d). The Kelvin waves in the zonal winds (Figure 12a) near the equator are generated at altitudes above 80 km, and such waves also appear in m = 2 (not shown). It is not known how these fast Kelvin waves are produced, but we suspect that the diurnal and semi-diurnal tides might be involved. As shown in Figure 12, eastward and westward propagating Rossby waves appear respectively in the winter and summer hemispheres throughout the region. In Figure 12, the westward propagating meridional winds hat peak near the equator (b), and the zonal winds that straddle the equator above 90 km (a) have the properties of Rossby gravity waves. Their amplitudes, however, are much smaller than those of the 2-day waves for m = 3 (Figure 10).

VI. Summary and Conclusions

We presented the results of a modeling study, which shows that the NSM produces PWs that have amplitudes in the mesosphere comparable to those observed. As in the model simulations of the middle atmosphere by Norton and Thuburn (1996, 1999), the PWs were purely generated by internal instabilities. No source of any kind was prescribed to excite the waves, neither thermal nor through momentum forcing. Of critical importance is the mean zonal circulation (m = 0), which creates the dynamical condition for generating the PWs. When we artificially suppress the solar heating that drives the mean zonal circulation and associated variations in temperature and pressure, the PWs essentially disappear. In addition to the seasonal variations in the solar UV heating that drives the middle atmosphere, the model also applies a tropospheric

heat source that qualitatively reproduces the observed zonal jets near the tropopause. This source proves to be significant in generating the long period planetary waves, in particular those for zonal wave numbers m = 1 and 2, which are involved to produce the non-migrating tides in the upper mesosphere. When the model is run without the excitation of the solar tides, the PWs are different but not the amplitudes in general.

The PWs in the NSM are highly variable but reveal systematic seasonal variations that could be caused by a number of processes not yet fully understood. Foremost of all is the dynamical state of the zonal mean (m = 0), which is conducive to create instabilities. In the mesosphere, the observed reversals in the zonal circulation and latitudinal temperature variations, due to gravity wave drag (Lindzen, 1981), can cause baroclinic instabilities to develop (Plumb, 1983). A similar condition could arise near the tropopause where zonal jets form and the latitudinal temperature variations reverse. The PWs thus generated by instabilities are amplified by GWs (Mayr et al., 2001), and they are filtered by the zonal circulation.

Three classes of PW are generated in the model:

(1) Rossby waves. These are waves that slowly propagate westward relative to the moving medium. Carried by the zonal jets in the middle atmosphere, these waves then appear to propagate relative to the ground eastward in winter and westward in summer.

(2) Rossby gravity waves. These waves are largely confined to low latitudes and the most prominent manifestations are the 2-day waves for m = 3. They occur primarily during solstice conditions where the temperature and pressure gradients across the equator are largest so that baroclinic instabilities develop (e.g., Plumb, 1983).

(3) Kelvin waves. These waves appear at high altitudes above 80 km in the zonal winds near the equator for m = 1 and 2 (not shown). The origin is not known but we believe that the diurnal and semi-diurnal tides might be involved.

References

Akmaev, R. A., Simulation of large-scale dynamics in the mesosphere and lower thermosphere with the Doppler-spread parameterization of gravity waves: 1. Implementation and zonal mean climatologies, *J. Geophys. Res.*, **106**, 1193, 2001.

Burks, D., and C. Leovy, Planetary waves near the mesospheric easterly jet, *Geophys. Res. Lett.*, **13**, No. 3, 193, 1986.

Chan, K. L., H. G. Mayr, J. G. Mengel, and I. Harris, A 'stratified' spectral model for stable and convective atmospheres, *J. Comp. Phys.*, **113**, 165, 1994.

Clark, R. R., A. C. Current, A. H. Manson et al., Global properties of the 2-day wave from mesosphere lower-thermosphere radar observations, *J. Atmos. Terr. Phys.*, **56**, 1279, 1994.

Craig, R. L., and W. G. Elford, Observations of the quasi 2-day wave near 90 km altitude at Adelaide (33° S), *J. Atmos. Terr. Phys.*, **43**, 1051, 1981.

Deng, W., J. E. Salah, R. R. Clark et al., Coordinated global radar observations of tidal and planetary waves in the mesosphere and lower thermosphere during January 20-30, 1993, *J. Geophys. Res.*, **102**, 7307, 1997.

Dunkerton, T. J., A two-dimensional model of the quasi-biennial oscillation, *J. Atmos. Sci.*, **42**, 1151 (1985).

Dunkerton, T. J., The role of gravity waves in the quasi-biennial oscillation, *J. Geophys. Res.*, **102**, 26053, 1997.

Forbes, J. M., and H. B. Garrett, Thermal excitation of atmospheric tides due to insolation absorption by O_3 and H_2O, *Geophys. Res. Lett.*, **5**, 1013, 1978.

Forbes, J. M., Tidal and planetary waves, *Geophysical Monograph* **87**, 67, 1995.

Fraser, G. J., G. Hernadez, and R. W. Smith, "Eastward moving 2-4 day waves in the winter antarctic mesosphere, *Geophys. Res. Lett.*, **20**, 1547, 1993.

Fritts, D. C., and J. R. Isler, Mean motion and tidal and 2-day structure and variability in the mesosphere and lower thermosphere, *J. Atmos. Sci.*, **51**, 2145, 1994.

Fritts, D., C., J. R. Isler, R. S. Lieberman et al., Two-day wave structure and mean flow interactions observed by radar and High Resolution Doppler Imager, *J. Geophys. Res.*, **104**, 3953, 1999.

Gray, L. J., and J. A. Pyle, A two dimensional model of the quasi-biennial oscillation of ozone, *J. Atmos. Sci.*, **46**, 203 (1989).

Harris, T. J., A long-term study of the quasi 2-day wave in the middle atmosphere, *J. Atm. Terr. Phys.*, **56**, 569, 1994.

Harris, T. J., and R. A. Vincent, The quasi-two-day wave observed in the equatorial middle atmosphere, *J. Geophys. Res.*, **98**, 10481, 1993.

Hays, P. B. et al. The high-resolution Doppler imager on the Upper Atmosphere Research Satellite, *J. Geophys. Res.*, **98**, 10,713, 1993.

Held, I. M., and A. Y. Hou, Nonlinear axially symmetric circulation in a near inviscid atmosphere, *J. Atmos. Sci.*, **37**, 515, 1980.

Hines, C. O., The saturation of gravity waves in the middle atmosphere. Part I: Critique of linear instability theory, *J. Atmos. Sci.*, **48**, 1348, 1991a.

Hines, C. O., The saturation of gravity waves in the middle atmosphere. Part II: Development of Doppler spread theory, *J. Atmos. Sci.*, **48**, 1360, 1991b.

Hines, C. O., Doppler-spread parameterization of gravity-wave momentum deposition in the middle atmosphere, 1, Basic formulation, *J. Atmos. Solar Terr. Phys.*, **59**, 371, 1997a.

Hines, C. O., Doppler-spread parameterization of gravity-wave momentum deposition in the middle atmosphere, 2, Broad and quasi monochromatic spectra, and implementation, *J. Atmos. Solar Terr. Phys.*, **59**, 387, 1997b.

Hines, C. O., Theory of the Eulerian tail in the spectra of atmospheric and oceanic internal gravity waves, *J. Fluid Mech.*, **448**, 289, 2001.

Hines, C. O., Nonlinearities and linearities in internal gravity waves of the atmosphere and the oceans, *Geophys. Astrophys. Fluid*, **96**, 1, 2002.

Holton, J. R., The generation of mesospheric planetary waves by zonally asymmetric gravity wave breaking, *J. Atmos. Sci.*, **41**, 3427, 1984.

Kinnersley, J. S., and S. Pawson, The descent rates of the shear zones of the equatorial QBO, *J Atmos. Sci.*, **53**, 1937 (1996).

Lindzen R. S. and J. R. Holton, A theory of the quasi-biennial oscillation, *J. Atmos. Sci.*, **25**, 1095, 1968.

Lindzen R. S., Turbulence and stress due to gravity wave and tidal breakdown, *J. Geophys. Res.*, **86**, 9707, 1981.

Lindzen, R. S., and A. Y. Hou, Hadley circulations for zonally averaged heating centered off the equator, *J. Atmos. Sci.*, **45**, 4073, 1988.

Manzini, E., N. A. McFarlane, and C. McLandress, Impact of the Doppler spread parameterization the simulation of the middle atmosphere circulation using the MA/ECHAM4 general circulation model, *J. Geophys. Res.*, **102**, 25,751, 1997.

Mayr, H. G, J. G. Mengel, C. O. Hines, K. L. Chan, N. F. Arnold, C. A. Reddy, and H. S. Porter, The gravity wave Doppler spread theory applied in a numerical spectral model of the middle atmosphere, 2, Equatorial oscillations, *J. Geophys. Res.*, **102**, 26093 (1997).

Mayr, H. G., J. G. Mengel, K. L. Chan, and H. S. Porter, Mesosphere dynamics with gravity forcing: Part I, Diurnal and semi-diurnal tides, *J. Atm. Solar-Terr. Phys.*, **63**, 1851, 2001a.

Mayr, H. G., J. G. Mengel, K. L. Chan, and H. S. Porter, Mesosphere dynamics with gravity forcing: Part II, Planetary waves, *J. Atm. Solar-Terr. Phys.*, 63, 1865, 2001b.

Meek, C. E., et al., Global study of northern hemisphere quasi 2-day wave events in recent summers near 90 km altitude, *J. Atm. Terr. Phys.*, **58**, 1401, 1996.

Mengel, J. G., H. G. Mayr, K. L. Chan, C. O. Hines, C. A. Reddy, N. F. Arnold, and H. S. Porter, Equatorial oscillations in the middle atmosphere generated by small scale gravity waves, *Geophys. Res. Lett.*, **22**, 3027, 1995.

Muller, H. G., and L. Nelson, A traveling quasi 2-day wave in the meteor region, *J. Atm. Terr. Phys.*, **40**, 761, 1978.

Mote, P. W. et al., An atmospheric tape recorder: The imprint of tropical tropopause temperatures on stratospheric water vapor, J. *Geophys. Res.*, **101**, 3989, 1996.

Norton, W. A., and J. Thuburn, The two-day wave in a middle atmosphere GCM, *Geophys. Res. Lett.*, **23**, 2113, 1996.

Norton, W. A., and J. Thuburn, Sensitivity of mesospheric mean flow, planetary waves and tides to strength of gravity wave drag, J. *Geophys. Res.*, **104**, 30,897, 1999.

Ffister, L., Baroclinic instability or easterly jets with application to the summer mesosphere, , *J. Atmos. Sci.*, **42**, 313, 1985.

Phillips, A., Simultaneous observations of the quasi 2-day wave at Manson, Antarctica, and Adelaide, South Australia, *J. Atm. Terr. Phys.*, **51**, 761, 1989.

Plumb, R. A., and A. Y. Hou, The response of a zonally symmetric atmosphere to subtropical thermal forcing: Threshold behavior, *J. Atmos. Sci.*, **49**, 1790, 1992.

Plumb, R. A., Baroclinic instability of the summer mesosphere: A mechanism for the quasi-2-day wave?, *J. Atmos. Sci.*, **40**, 262, 1983.

Plumb, R. A., R. A. Vincent, and R. L. Craig, The quasi-2-day wave event of January 1984 and its impact on the mean mesospheric circulation, *J. Atmos. Sci.*, **44**, 3030, 1987.

Poole, L. M. G., The characteristics of mesospheric two-day wave as observed at Grahamstown (33.3° S, 26.5° E), *J. Atm. Terr. Phys.*, **52**, 259, 1990.

Shepherd, G. G., et al., WINDII, the Wind Imager Interferometer on the Upper Atmosphere Research Satellite, *J. Geophys. Res.*, **98**, 10,7725, 1993.

Smith, A., K., Longitudinal variations in mesospheric winds: Evidence for gravity wave filtering by planetary waves, *J. Atmos. Sci.*, **53**, 1156, 1996.

Smith, A., K., Stationary planetary waves in upper mesospheric winds, *J. Atmos. Sci.*, **54**, 2129, 1997.

Strobel, D. F., Parameterization of atmospheric heating from 15 to 120 km due to O2 and O3 absorption of solar radiation, *J. Geophys. Res.*, **83**, 6225, 1978.

Tsuda, T., S. Kato, and R. A. Vincent, Long period oscillations observed by the Kyoto meteor radar and comparison of the quasi 2-day wave with Adelaide MF radar observations, *J. Atm. Terr. Phys.*, **50**, 225, 1988.

Volland, H., *Atmospheric Tidal and Planetary Waves*, Kluwer Academic Publ., Boston, MA, 1988.

Wang, D. W., W. E. Ward, G. G. Shepherd, and D. L. Wu, Stationary planetary waves inferred from WINDII wind data taken within altitudes 90-120 km during 1991-96, *J. Atmos. Sci.*, **57**, 1906, 2000.

Wehrbein, W. M., and C. B. Leovy, An accurate radiative heating and cooling algorithm for use in a dynamical model of the middle atmosphere, *J. Atmos. Sci.*, **39**, 1532, 1982.

Williams, P. J., N. J. Mitchell, A. G. Beard, V. S. Howells, and H. G. Muller, The coupling of planetary waves, tides, and gravity waves in the mesosphere and lower thermosphere, *Adv. Space Res.*, **24**, 1571, 1999.

Wu, D. L., P. B. Hays, W. R. Skinner et al., Observations of the quasi 2-day wave from the High Resolution Doppler Imager on UARS, *Geophys. Res. Lett.*, **20**, 2853, 1993.

Zhu, X, Radiative cooling calculated by random band models with S-1-beta tailed distribution, *J. Atmos. Sci.*, **46**, 511, 1989.

Figure Captions

Figure 1: Zonal-mean (m = 0) temperature perturbations (a) and zonal winds (b), which are computed with the tropospheric heat source. The reversals in the latitudinal temperature gradients around the tropopause and around 65 km are conducive to create the instabilities that produce the PWs in the NSM.

Figure 3: Equatorial oscillations generated by GWs. The QBO period is close to 28 months, close to the middle of observed values, but the amplitudes are relatively small. (No attempt was made to tune the model with GW parameters to reproduce a more realistic QBO).

Figure 3: Schematic, illustrating the dynamical features and processes involved in generating the PWs. In the mean zonal circulation (m = 0), which includes the jets near the tropopause, the PWs are generated by instabilities, and they are modified by filtering. The non-migrating tides in the NSM are produced by non-linear coupling between migrating tides and PWs. As enumerated, GW interactions cause in the mesosphere reversals in the zonal winds and temperature variations. The PWs (and tides) are amplified by the GWs.

Figure 4: Zonal wind (a) and temperature perturbations (b) of PWs for m = 1 to 4 at 90 km altitude and 48° latitude, computed over a time span of 2 years with the standard model that includes the tropospheric source. Note the persistent seasonal variations, e.g., the short period (2 to 3 days) waves during summer months for m = 3 and 4, and the long period waves during spring and fall in particular for m = 1 and 2.

Figure 5: (a) Analogous to Figure 4a but computed without the tropospheric heat source. Compared to the standard model with the tropospheric source (Figure 4a), the short period waves for m = 3 and 4 are similar in magnitude, but the amplitudes of the long period waves are significantly smaller in particular for m = 1 and 2. This affects significantly the non-migrating tides as shown in Figure 6. (b) Analogous to Figure 4a but computed without a heat source for m = 0 throughout the atmosphere. Although PWs are generated, e.g. for m = 2, their amplitudes are generally negligibly small (note the differences in scales).

Figure 6: Amplitudes of the m = 0 non-migrating diurnal tide at 100 km altitude and 18° latitude, computed with (a) and without (b) the tropospheric heat source. This tide is generated through non-linear coupling involving the long-period m = 1 PWs. The differences (a compared to b) are large, which is consistent with the differences between the PWs shown in Figures 4a and 5a. Analogous to (a, b) but for the m = 1 non-migrating semi-diurnal tide at 84° latitude (c, d), which is also generated with m = 1 PWs.

Figure 7: Meridional wind (a) and temperature perturbations (b) of PWs for m = 3 at 4° latitude and at different altitudes from 20 to 90 km. The short period waves dominate during summer and winter months, except at 20 km where the long period waves are more prominent.

Figure 8: Contour plot of meridional winds for PWs with m = 3 at 60 km (a) and 90 km (b) altitudes. To reveal the seasonal variations, the contours below 50% of the maximum amplitudes are suppressed, but the maxima are quoted (27 m/s in each case). Note the systematic seasonal variations, which shows that the PWs are more prevalent during winter months at 60 km (a), but extend across the equator into the summer hemisphere at 90 km (b).

Figure 9: Spectra of m = 3 PWs propagating eastward (solid lines) and westward (dashed) for the zonal (a) and meridional (b) winds at 60 km derived from a short time span of 2 months following solstice with the sun in the southern hemisphere. In the Fourier analysis, running windows are applied that are a factor 3 larger than the derived periods. To suppress chaff, the lowest 20% of the contour maxima are suppressed, but the maximum amplitudes are stated. Note the eastward propagating waves in the winter hemisphere where the zonal jets are directed eastward (Figure 1), and the westward propagating waves in the summer hemisphere where the zonal jets are directed westward. At mid latitudes, these are Rossby waves that slowly propagate westward relative to the moving medium they are embedded in. Their apparent propagation velocities are significantly affected (Doppler shifted) by the zonal winds. Westward propagating Rossby gravity waves are characterized by the meridional wind maxima near the equator and zonal wind maxima that tend to straddle the equator. Analogous to (a) and (b), the zonal (c) and meridional winds (d) are presented at 90 km. This shows that the largest PWs occur in the summer hemisphere, which is consistent with the trend seen in Figure 8.

Figure 10: Height variations of m = 3 PWs with periods between 2 and 4 days, which bears on the results presented in Figure 9. It shows the Rossby waves at mid latitudes, eastward in winter and westward in summer, and the westward propagating Rossby gravity waves at low latitudes. Around 65 km the wave activity is concentrated in the winter hemisphere, but higher up the waves are more prevalent in the summer hemisphere as Figure 8 shows.

Figure 11: Spectra for m = 1 PWs at 60 km (a, b) and 100 km (c, d) altitudes. Note that for m = 1, the waves do not vanish at the poles, unlike those for m > 1. Both eastward and westward propagating Rossby waves are shown at 60 km in the winter and summer hemispheres respectively. The zonal winds near the equator (c) are the signatures of Kelvin waves. The Mercator projection is applied to expand the regions at high latitudes where the waves are prominent.

Figure 12: Height variations of m = 1 PWs with periods from 2 to 4 days (a, b) and from 4 to 10 days (c, d). At mid to high latitudes, Rossby waves are present. Above 80 km, Kelvin waves appear in the zonal winds. Signatures of westward propagating Rossby gravity waves are seen in the meridional winds (b) around the equator and in the zonal winds that straddle the equator above 90 km (a). The amplitudes of the long period Rossby waves (c, d) are larger than those for shorter periods (a, b). The Mercator projection is again applied.

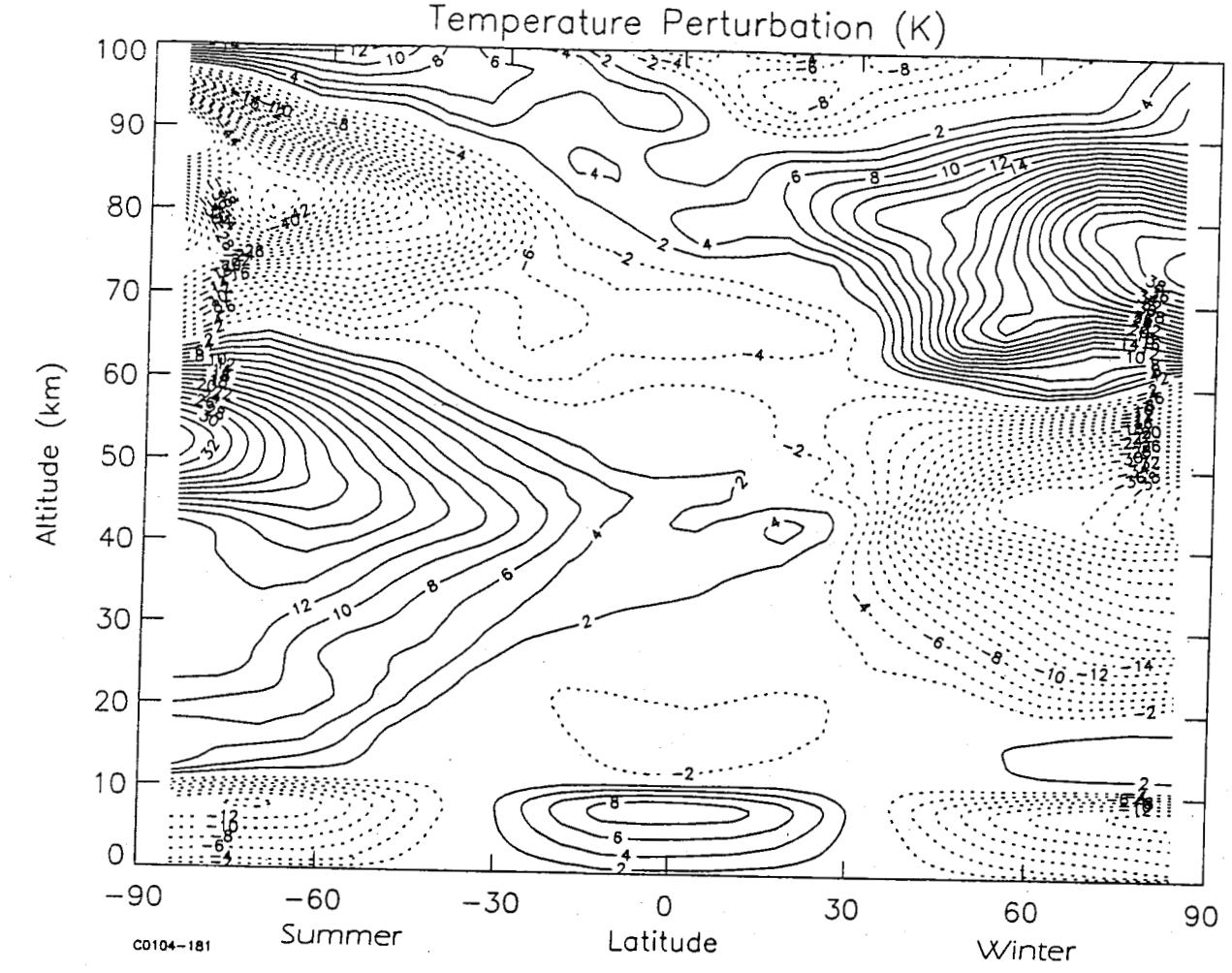
Temperature Perturbation (K)
Altitude (km)
100
90
80
70
60
50
40
30
20
10
0
-90
-60
-30
0
30
60
90
Summer
Latitude
Winter
C0104-181

a

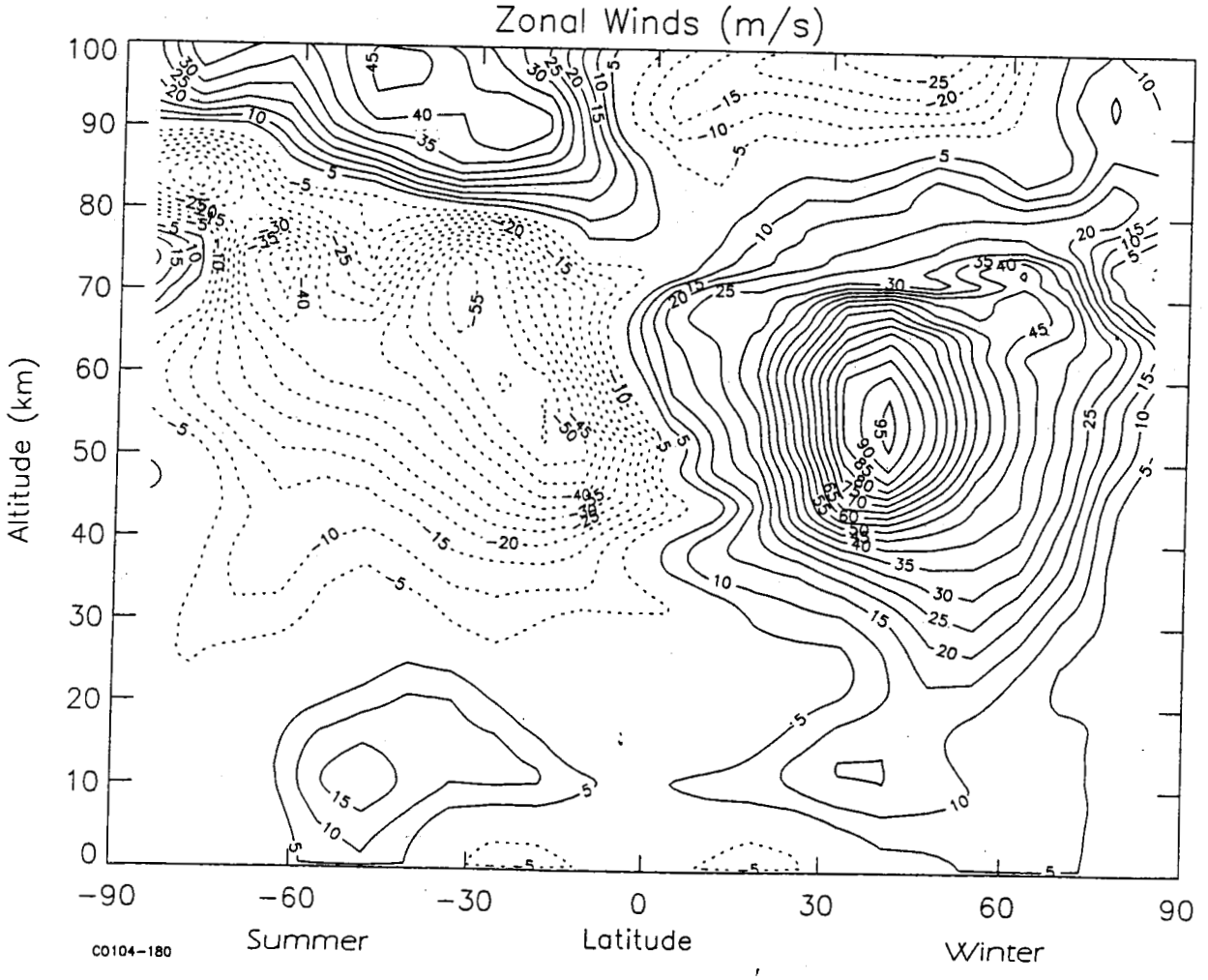
Zonal Winds (m/s)
Altitude (km)
100
90
80
70
60
50
40
30
20
10
0
-90
-60
-30
0
30
60
90
Summer
Latitude
Winter
C0104-180

b

Figure 1

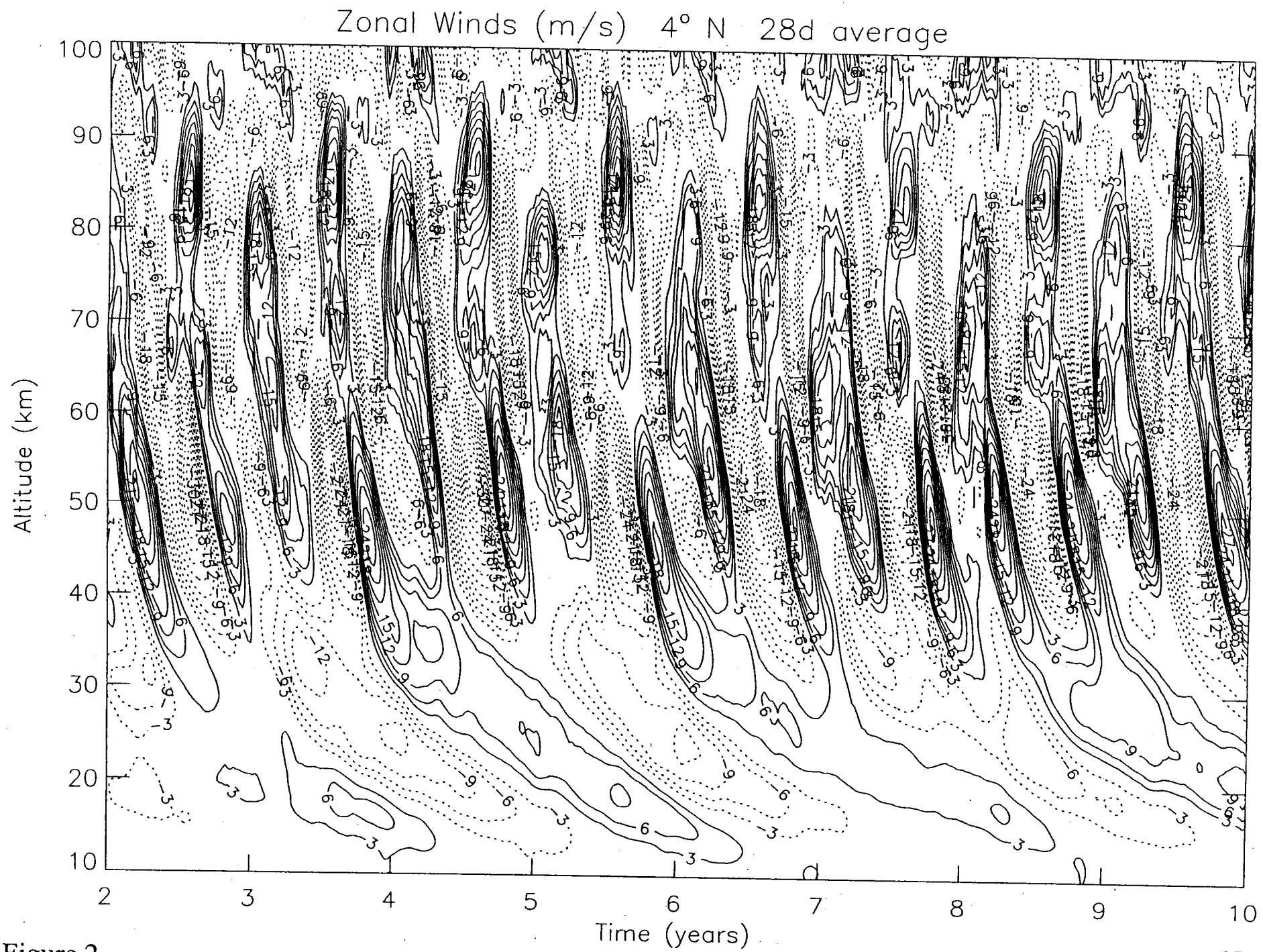
Zonal Winds (m/s) 4° N 28d average
Altitude (km)
100
90
80
70
60
50
40
30
20
10
2
3
4
5
6
7
8
9
10
Time (years)

Figure 2

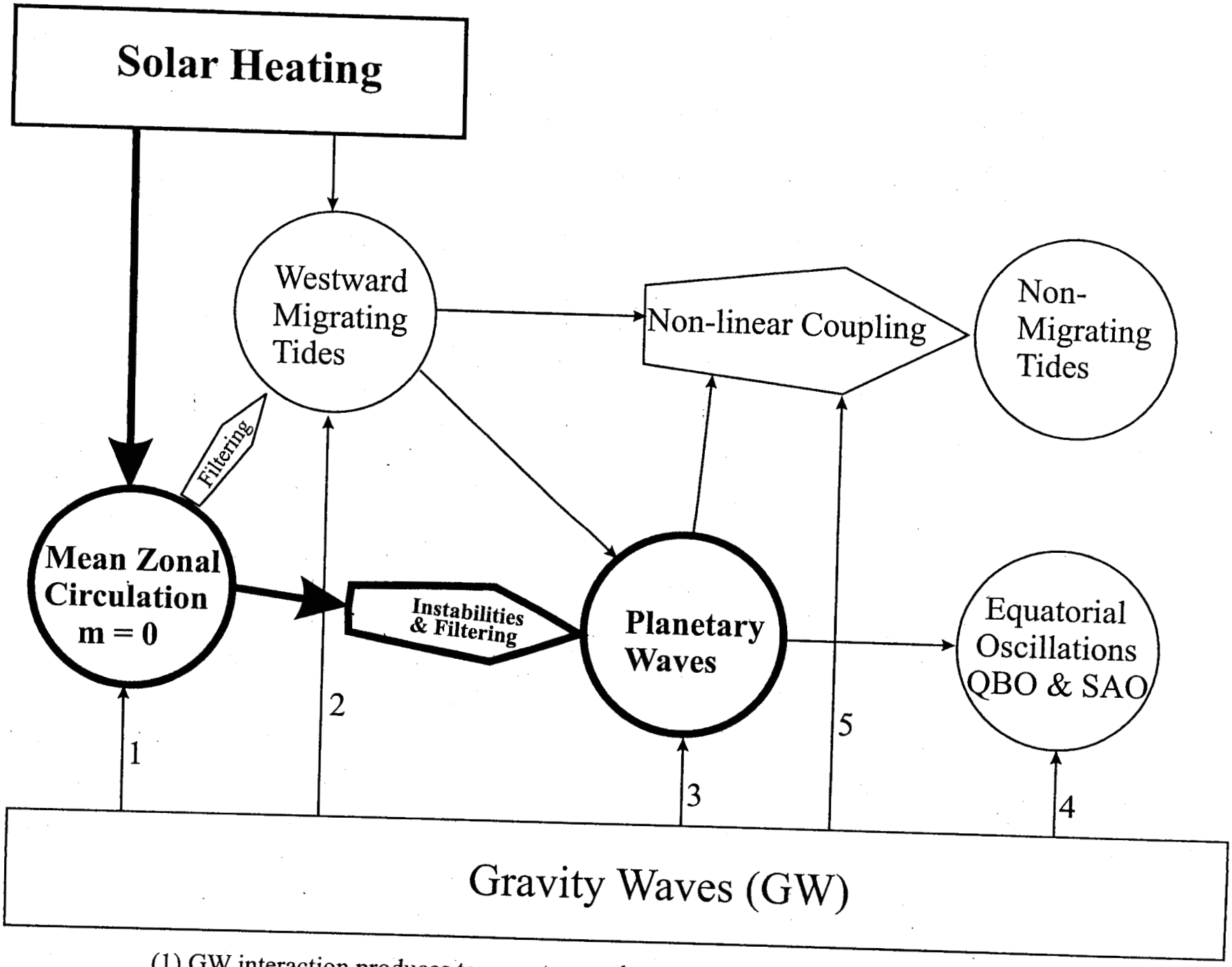

Figure 3

(1) GW interaction produces temperature and wind reversals that lead to instabilities
(2) GW interaction amplifies tides
(3) GW interaction amplifies planetary waves
(4) GW source of QBO and SAO
(5) GW filtering contributes to non-linear coupling

With Tropospheric Zonal Mean (m = 0) Heat Source

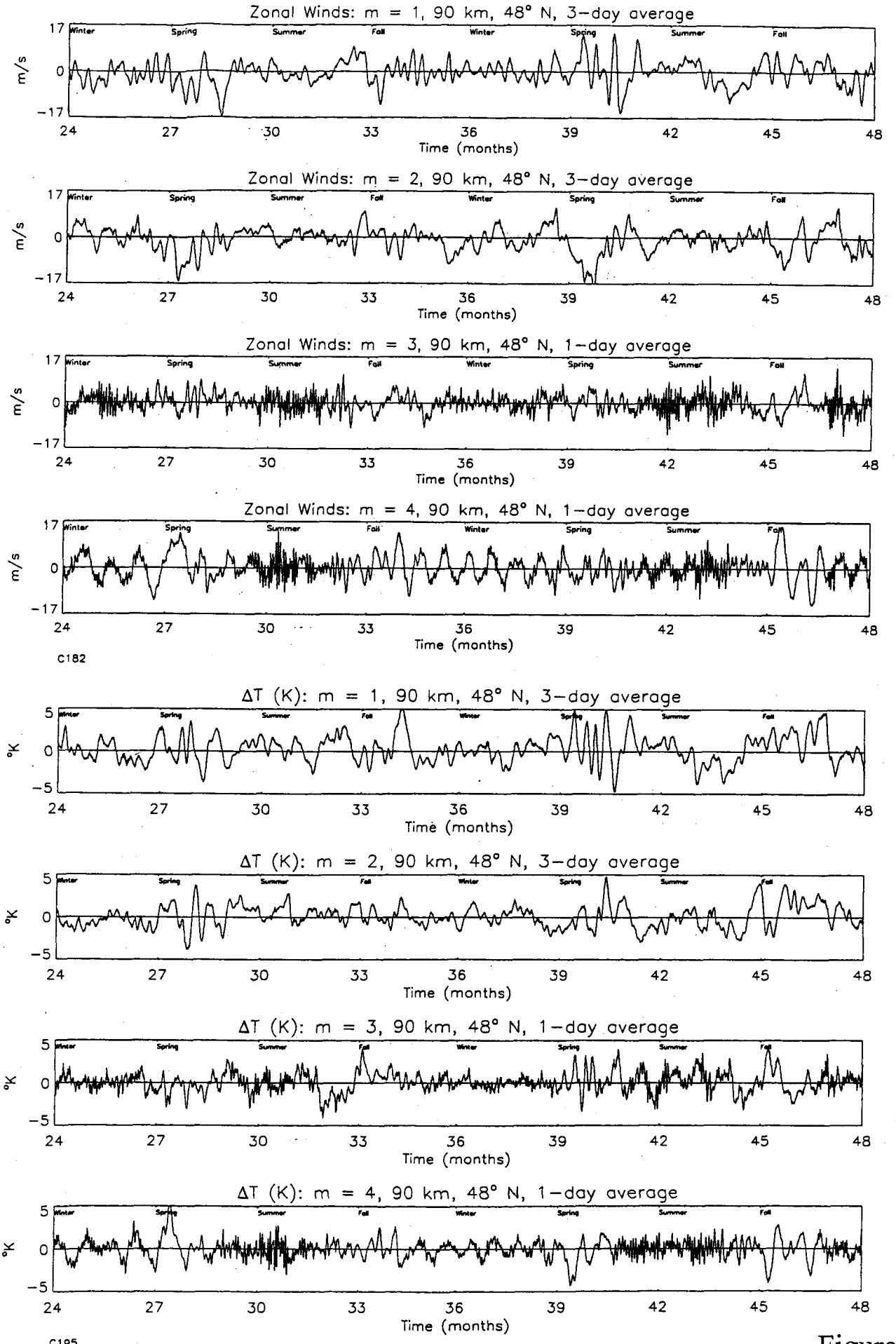

a

b

Figure 4

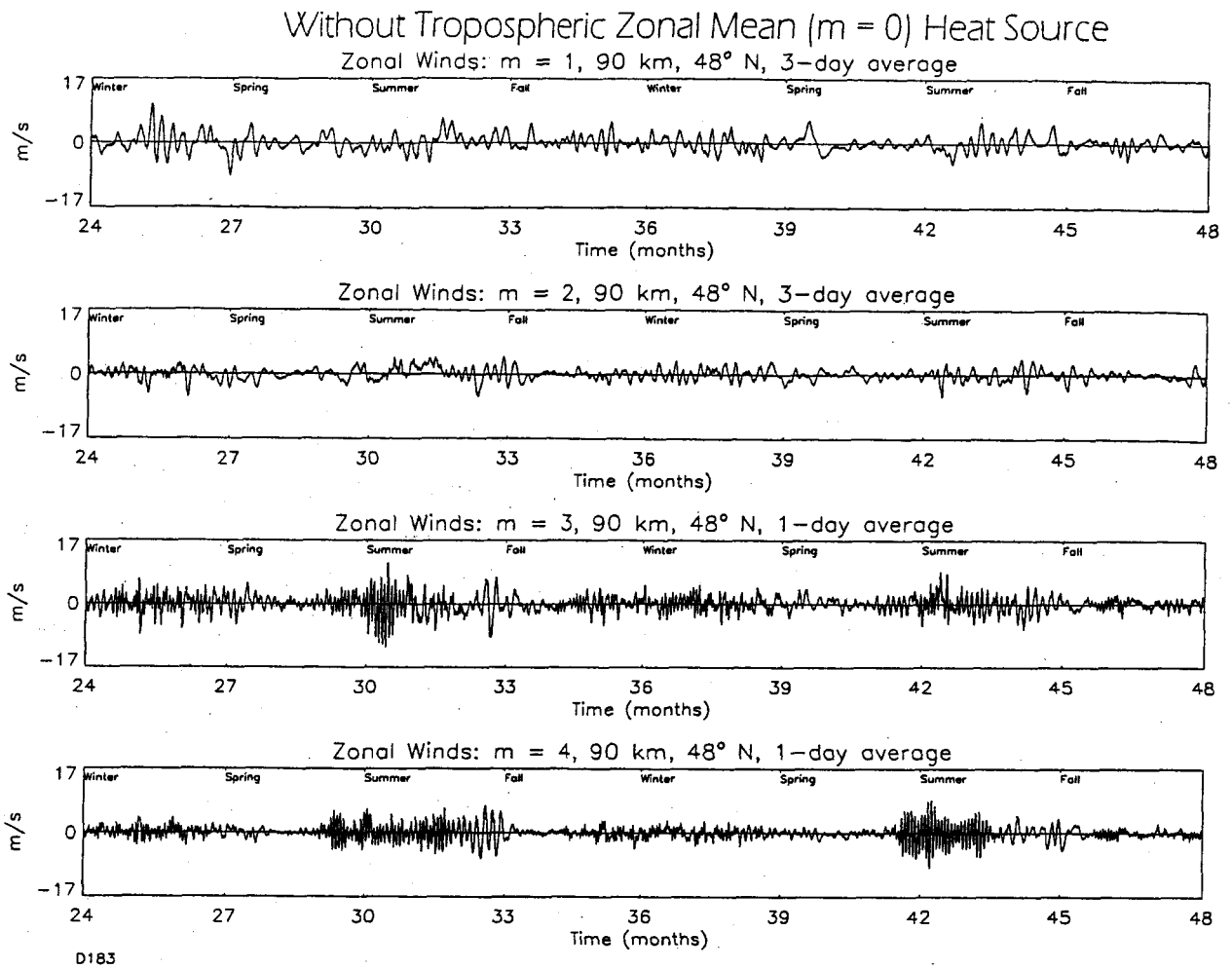
Without Tropospheric Zonal Mean (m = 0) Heat Source
Zonal Winds: m = 1, 90 km, 48° N, 3-day average
Zonal Winds: m = 2, 90 km, 48° N, 3-day average
Zonal Winds: m = 3, 90 km, 48° N, 1-day average
Zonal Winds: m = 4, 90 km, 48° N, 1-day average
Winter
Spring
Summer
Fall
m/s
Time (months)
D183

a

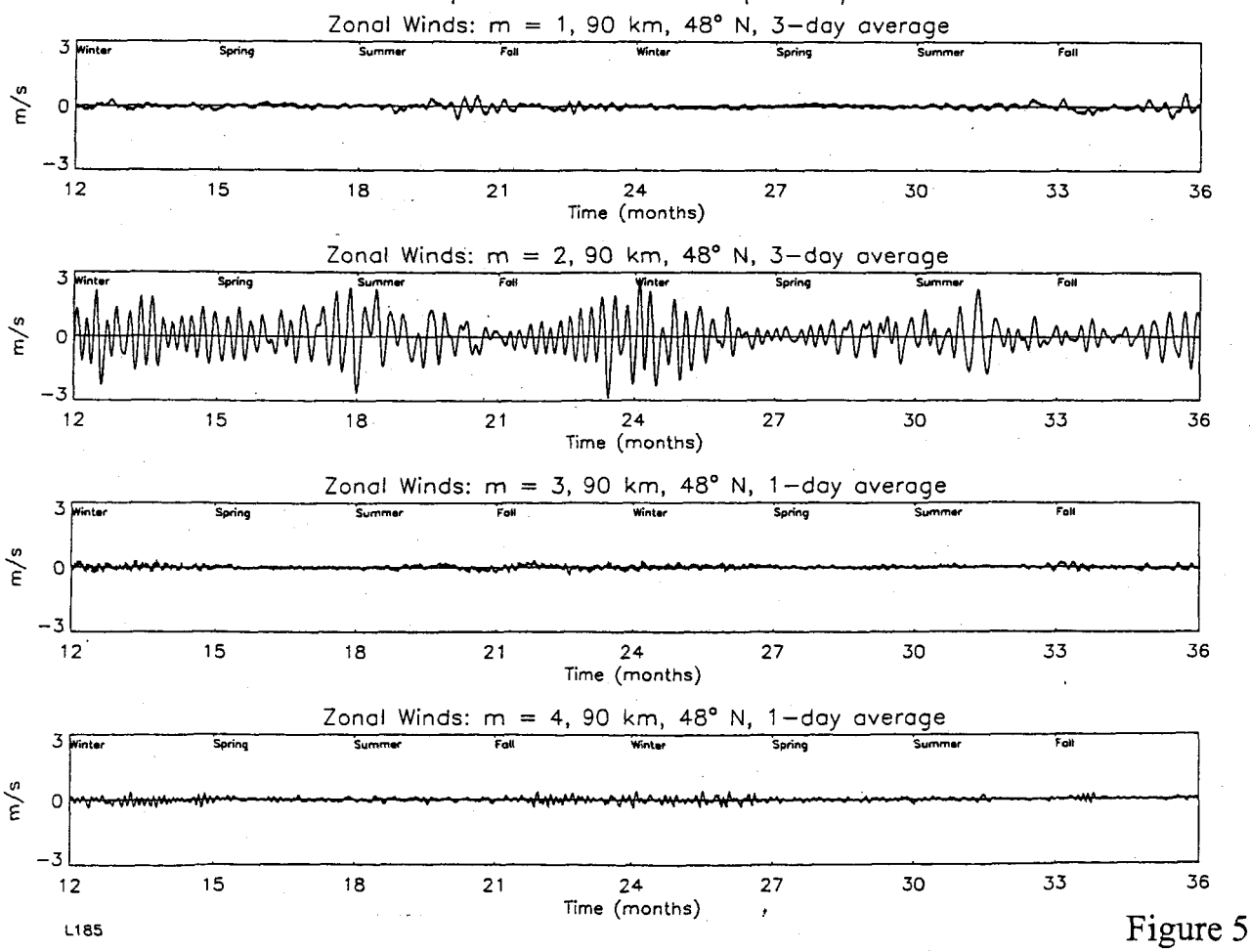
Without Atmospheric Zonal Mean (m = 0) Heat Source
Zonal Winds: m = 1, 90 km, 48° N, 3-day average
Zonal Winds: m = 2, 90 km, 48° N, 3-day average
Zonal Winds: m = 3, 90 km, 48° N, 1-day average
Zonal Winds: m = 4, 90 km, 48° N, 1-day average
Winter
Spring
Summer
Fall
m/s
Time (months)
L185

b

Figure 5

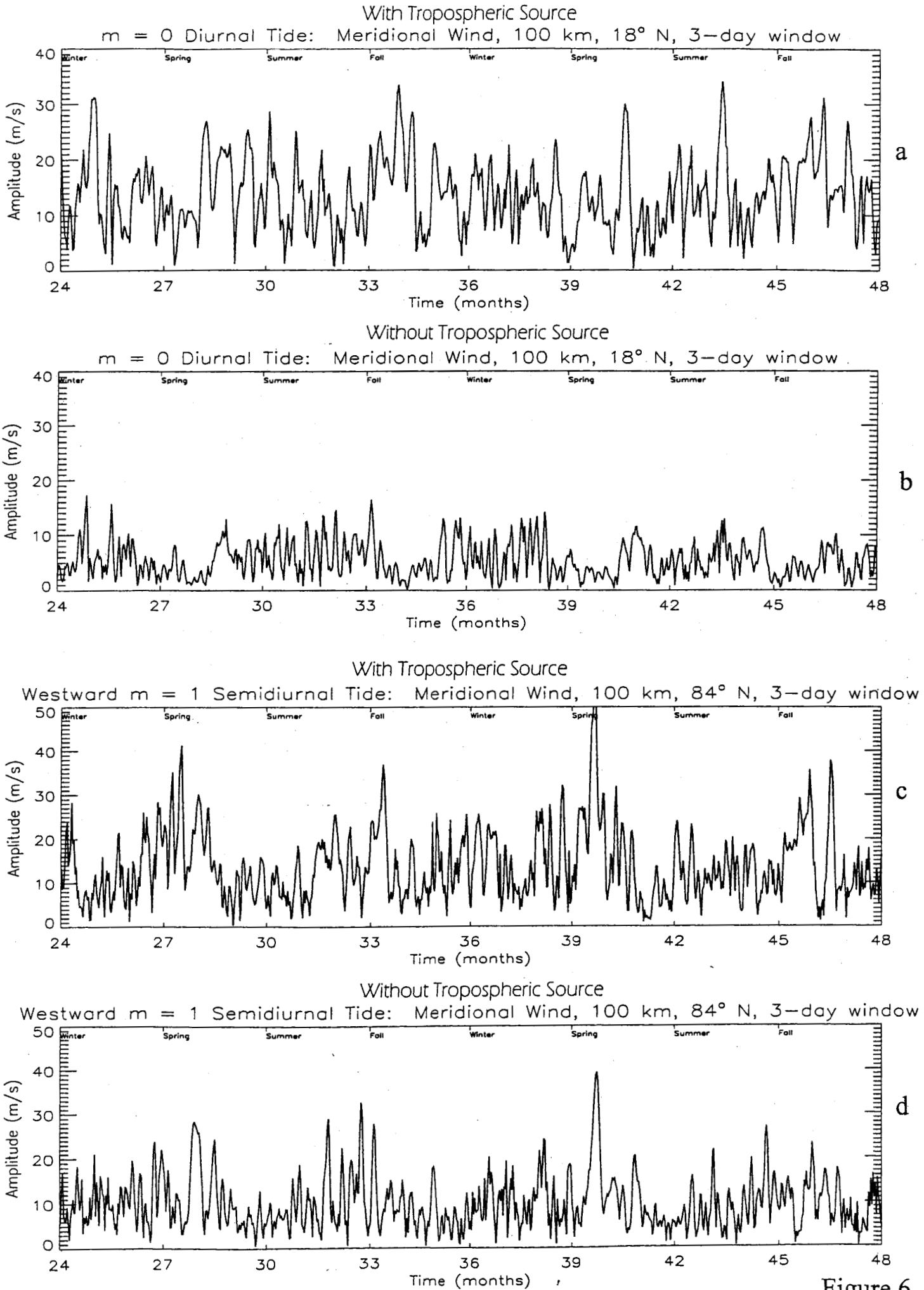
With Tropospheric Source
m = 0 Diurnal Tide: Meridional Wind, 100 km, 18° N, 3−day window
Winter
Spring
Summer
Fall
Amplitude (m/s)
Time (months)
a
Without Tropospheric Source
m = 0 Diurnal Tide: Meridional Wind, 100 km, 18° N, 3−day window
b
With Tropospheric Source
Westward m = 1 Semidiurnal Tide: Meridional Wind, 100 km, 84° N, 3−day window
c
Without Tropospheric Source
Westward m = 1 Semidiurnal Tide: Meridional Wind, 100 km, 84° N, 3−day window
d

Figure 6

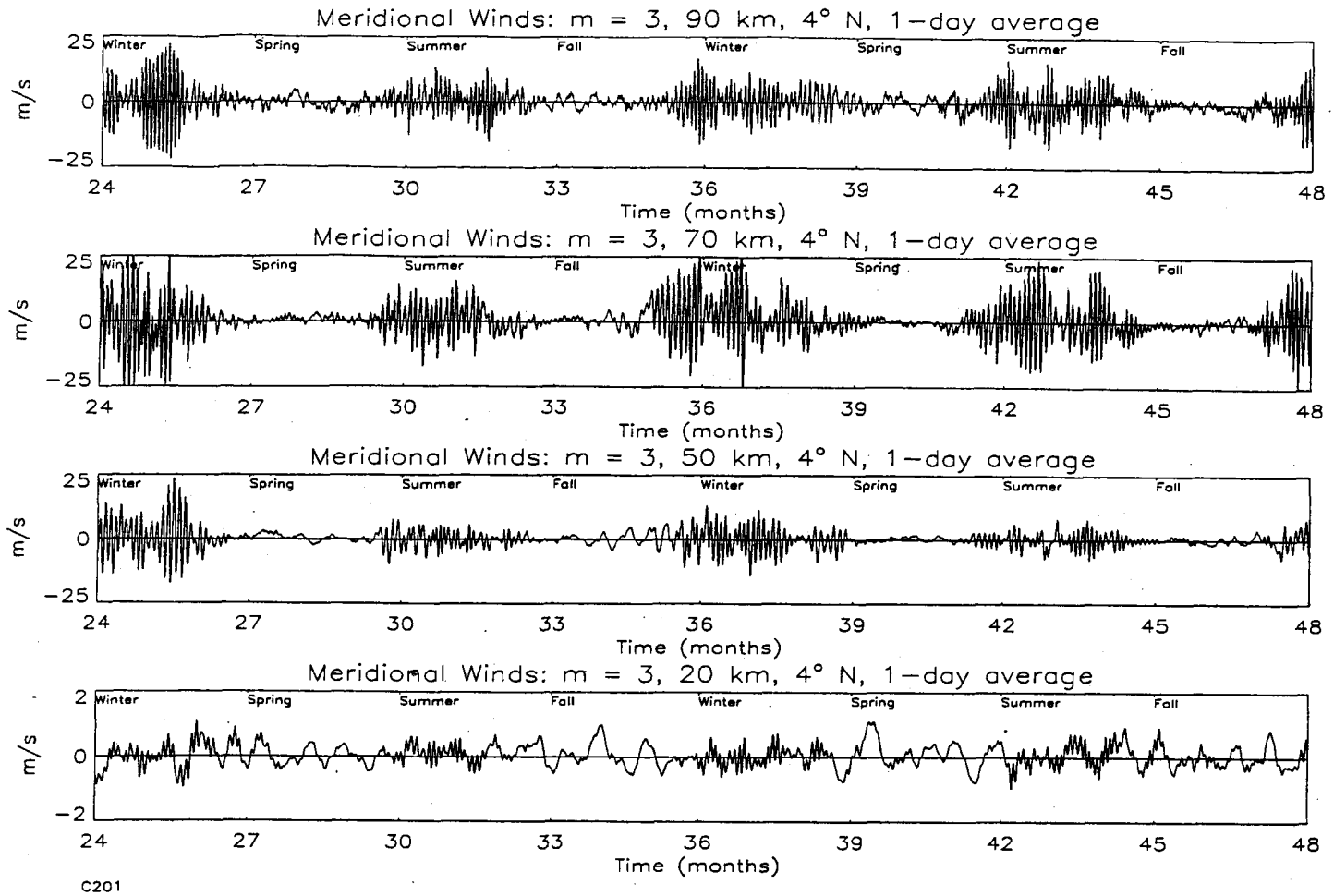
Meridional Winds: m = 3, 90 km, 4° N, 1−day average
Meridional Winds: m = 3, 70 km, 4° N, 1−day average
Meridional Winds: m = 3, 50 km, 4° N, 1−day average
Meridional Winds: m = 3, 20 km, 4° N, 1−day average
Winter
Spring
Summer
Fall
m/s
Time (months)
C201

a

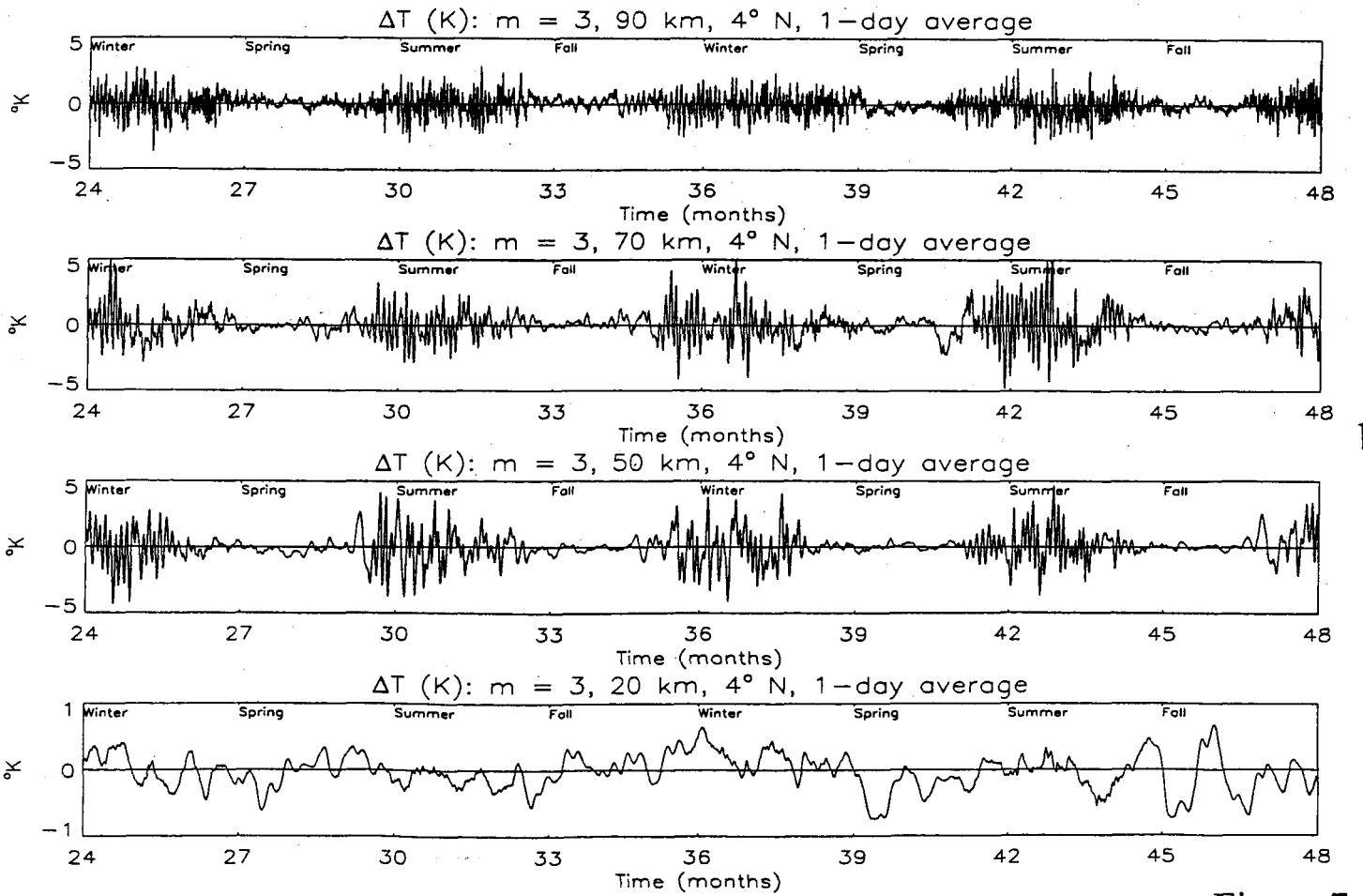
ΔT (K): m = 3, 90 km, 4° N, 1−day average
ΔT (K): m = 3, 70 km, 4° N, 1−day average
ΔT (K): m = 3, 50 km, 4° N, 1−day average
ΔT (K): m = 3, 20 km, 4° N, 1−day average
Winter
Spring
Summer
Fall
°K
Time (months)
C202

b

Figure 7

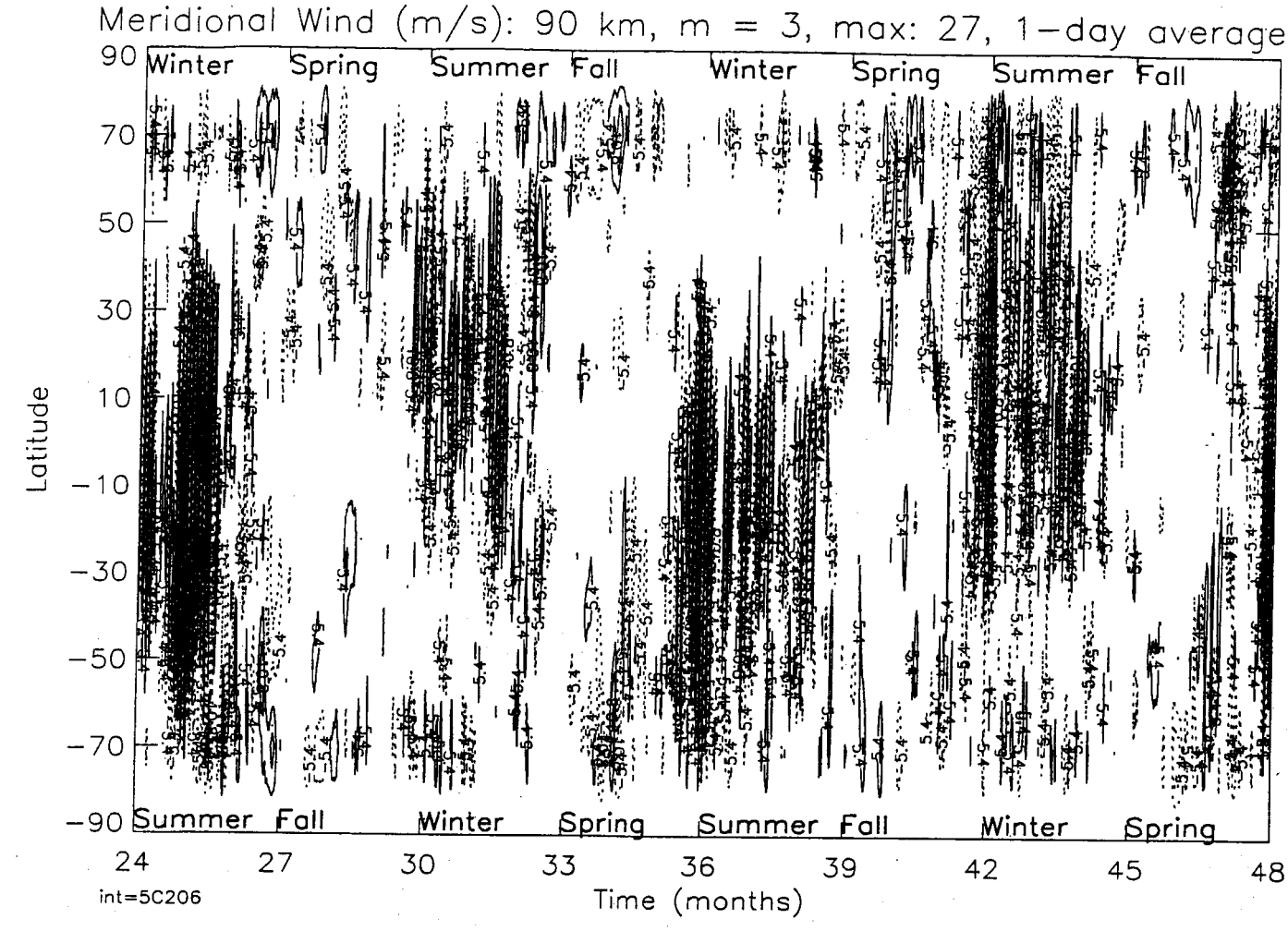
Meridional Wind (m/s): 90 km, m = 3, max: 27, 1-day average
Winter
Spring
Summer
Fall
Winter
Spring
Summer
Fall
Latitude
90
70
50
30
10
−10
−30
−50
−70
−90
Summer
Fall
Winter
Spring
Summer
Fall
Winter
Spring
24
27
30
33
36
39
42
45
48
int=5C206
Time (months)

b

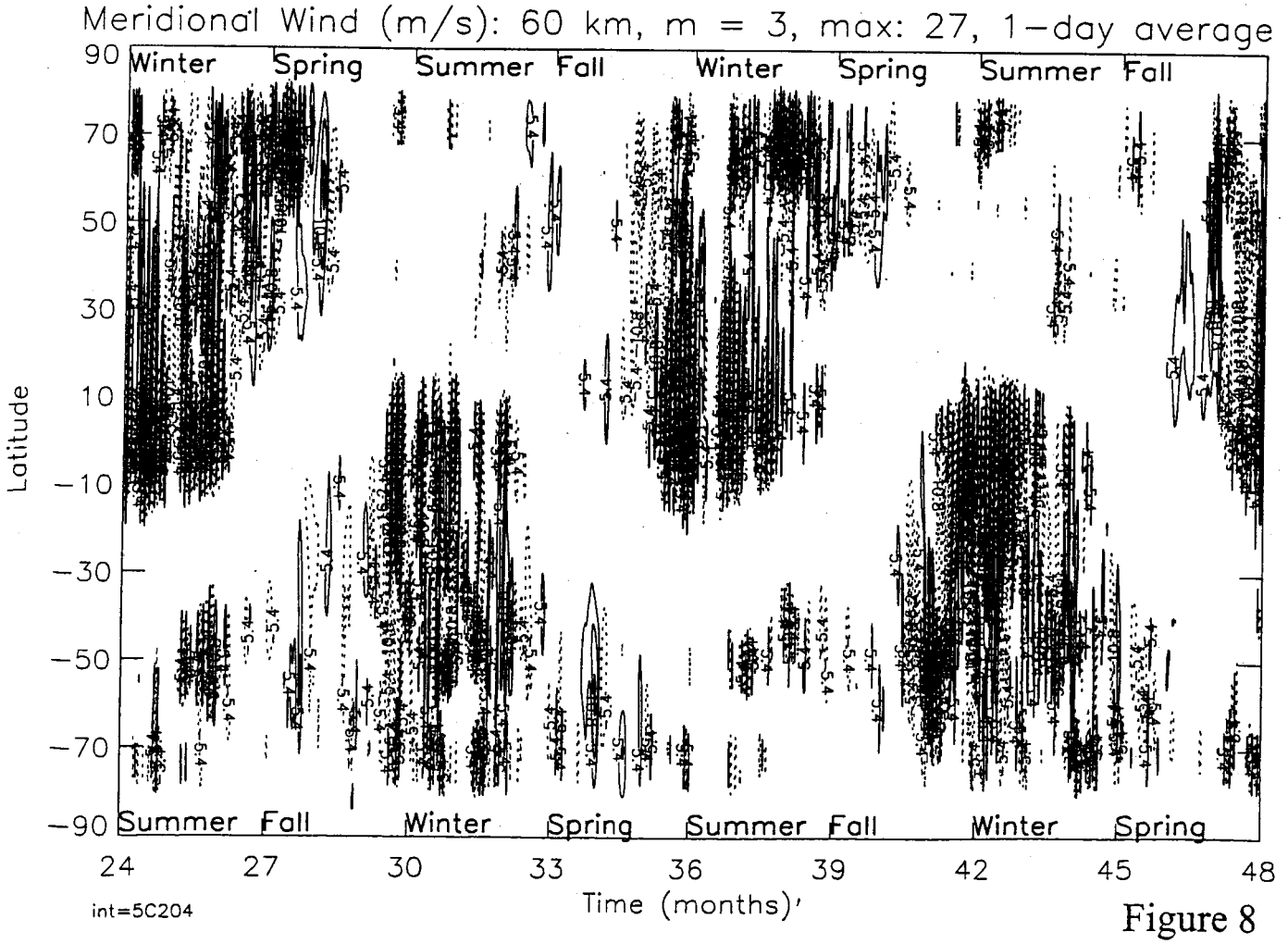
Meridional Wind (m/s): 60 km, m = 3, max: 27, 1-day average
Winter
Spring
Summer
Fall
Winter
Spring
Summer
Fall
Latitude
90
70
50
30
10
−10
−30
−50
−70
−90
Summer
Fall
Winter
Spring
Summer
Fall
Winter
Spring
24
27
30
33
36
39
42
45
48
int=5C204
Time (months)

a

Figure 8

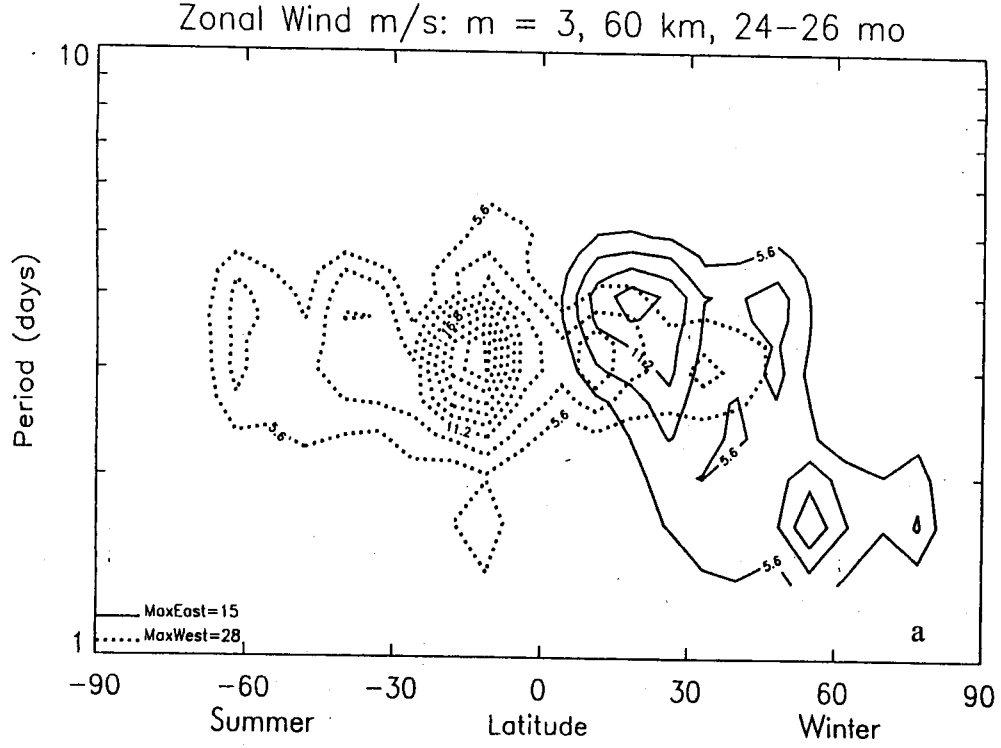
Zonal Wind m/s: m = 3, 60 km, 24–26 mo
Period (days)
10
1
MaxEast=15
MaxWest=28
a
−90
−60
−30
0
30
60
90
Summer
Latitude
Winter

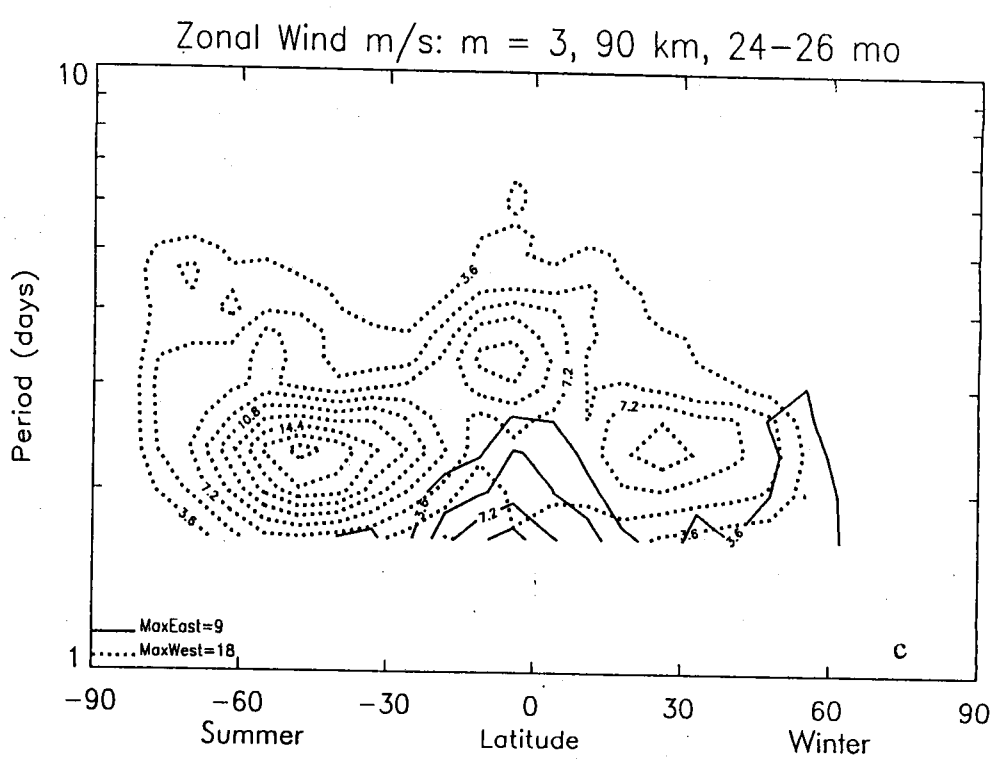
Zonal Wind m/s: m = 3, 90 km, 24–26 mo
Period (days)
10
1
MaxEast=9
MaxWest=18
c
−90
−60
−30
0
30
60
90
Summer
Latitude
Winter

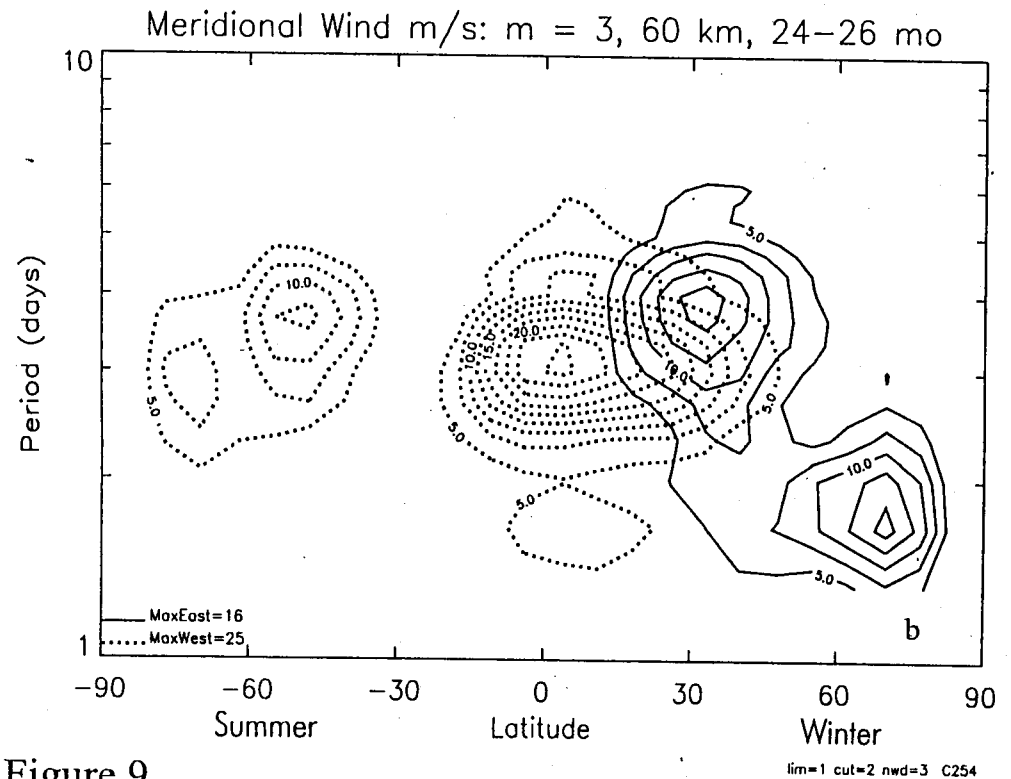
Meridional Wind m/s: m = 3, 60 km, 24–26 mo
Period (days)
10
1
MaxEast=16
MaxWest=25
b
−90
−60
−30
0
30
60
90
Summer
Latitude
Winter
lim=1 cut=2 nwd=3 C254

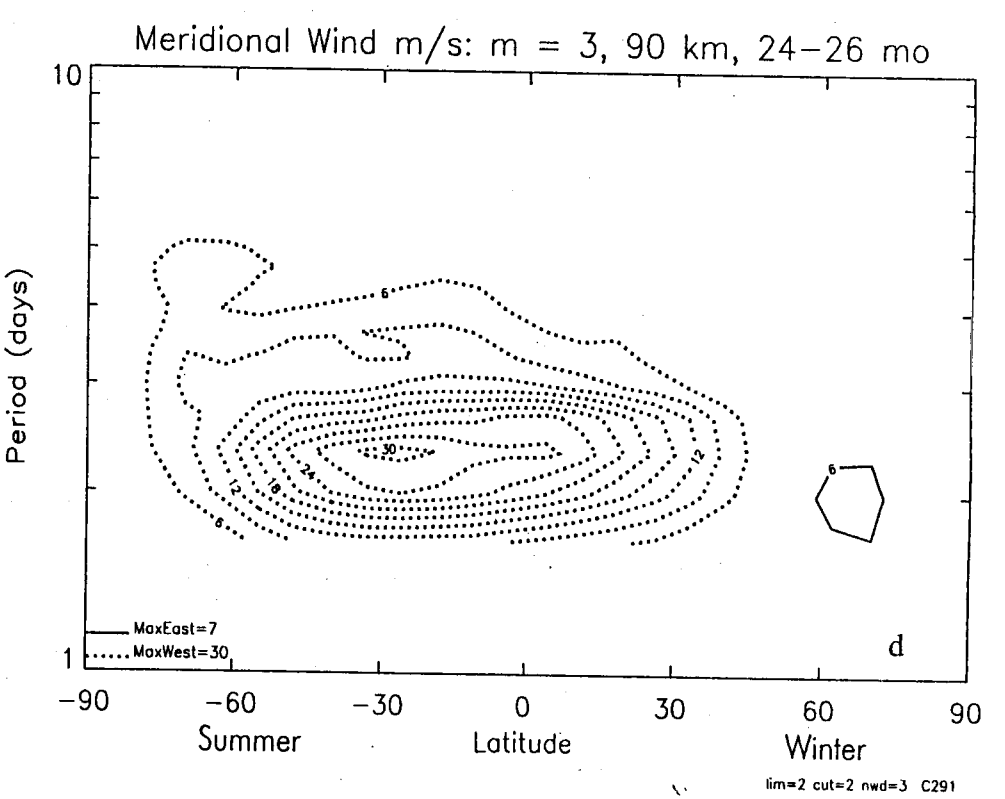
Meridional Wind m/s: m = 3, 90 km, 24–26 mo
Period (days)
10
1
MaxEast=7
MaxWest=30
d
−90
−60
−30
0
30
60
90
Summer
Latitude
Winter
lim=2 cut=2 nwd=3 C291

Figure 9

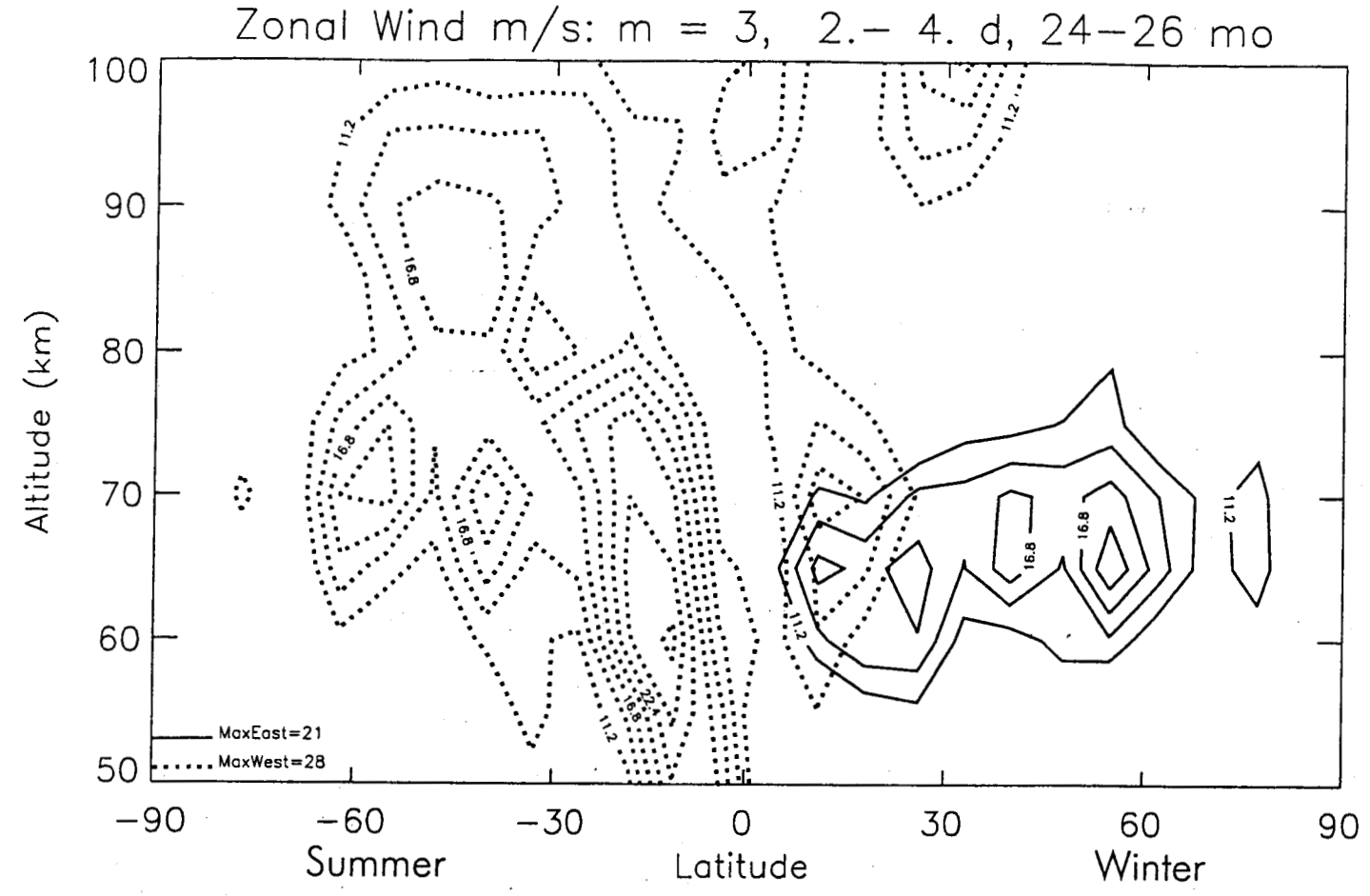
Zonal Wind m/s: m = 3, 2.– 4. d, 24–26 mo
Altitude (km)
100
90
80
70
60
50
11.2
16.8
22.4
MaxEast=21
MaxWest=28
−90
−60
−30
0
30
60
90
Summer
Latitude
Winter

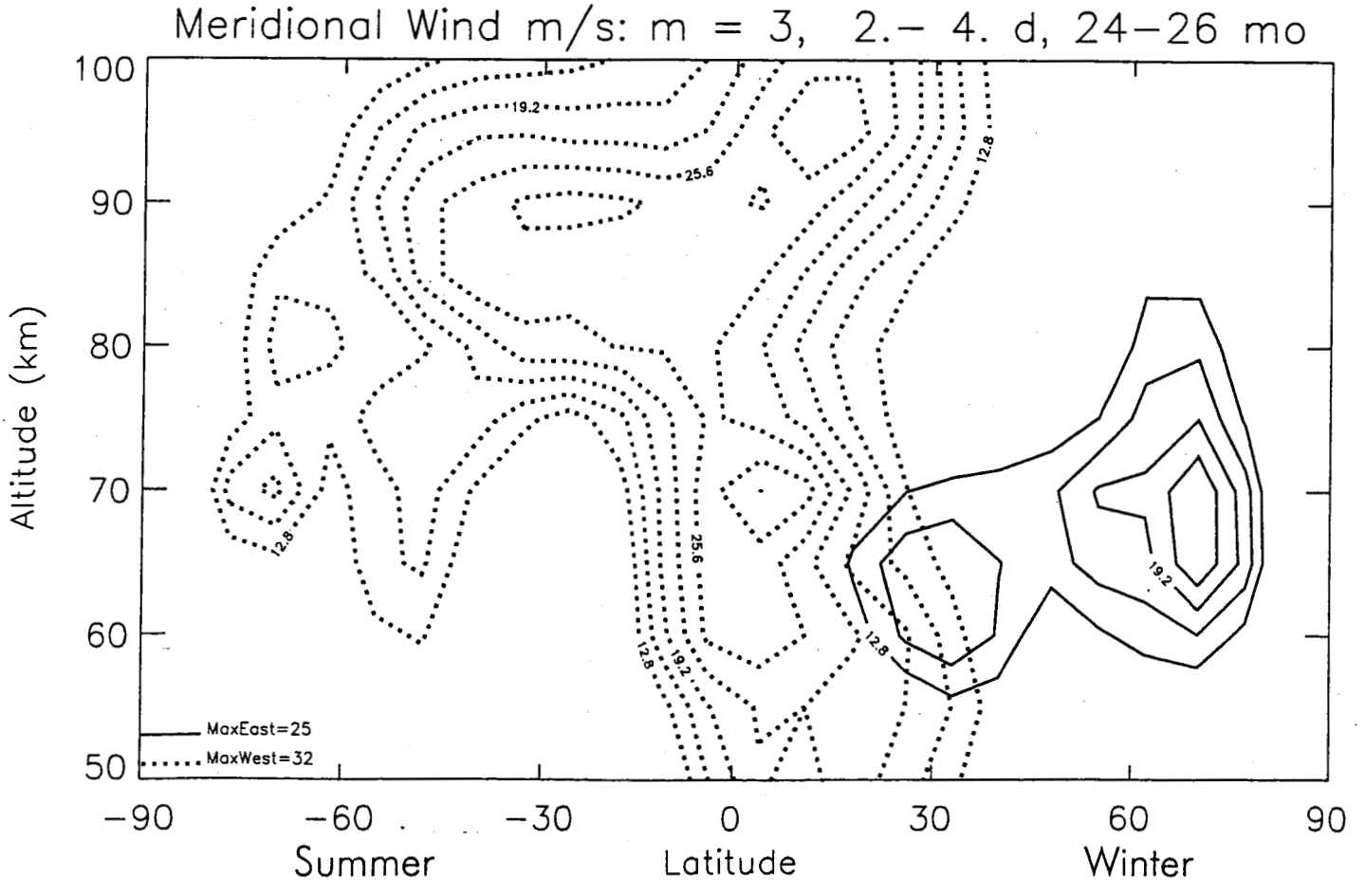
Meridional Wind m/s: m = 3, 2.– 4. d, 24–26 mo
Altitude (km)
100
90
80
70
60
50
12.8
19.2
25.6
MaxEast=25
MaxWest=32
−90
−60
−30
0
30
60
90
Summer
Latitude
Winter
cut=4 nwd=2 C249

Figure 10

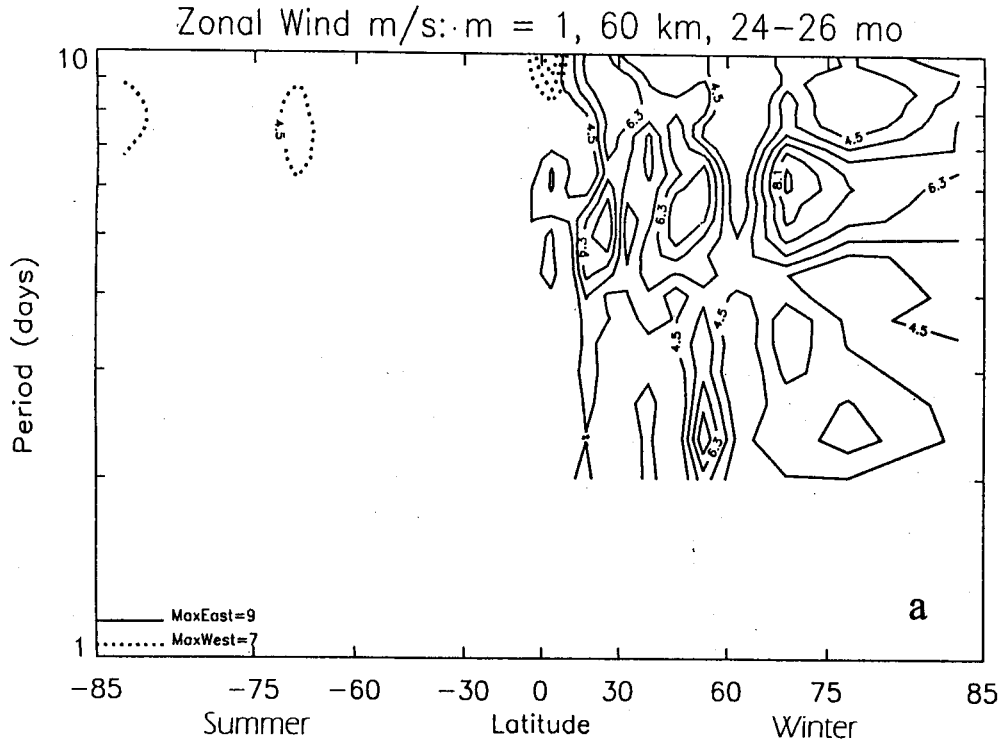
Zonal Wind m/s: m = 1, 60 km, 24–26 mo
Period (days)
10
1
MaxEast=9
MaxWest=7
a
−85 −75 −60 −30 0 30 60 75 85
Summer
Latitude
Winter

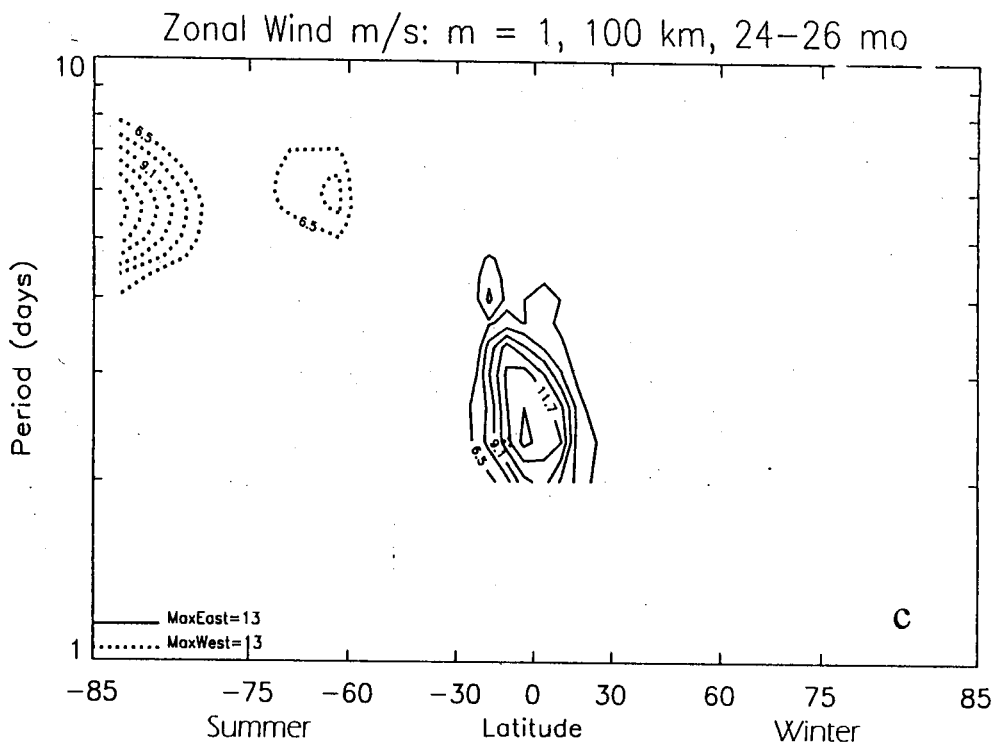
Zonal Wind m/s: m = 1, 100 km, 24–26 mo
Period (days)
10
1
MaxEast=13
MaxWest=13
c
−85 −75 −60 −30 0 30 60 75 85
Summer
Latitude
Winter

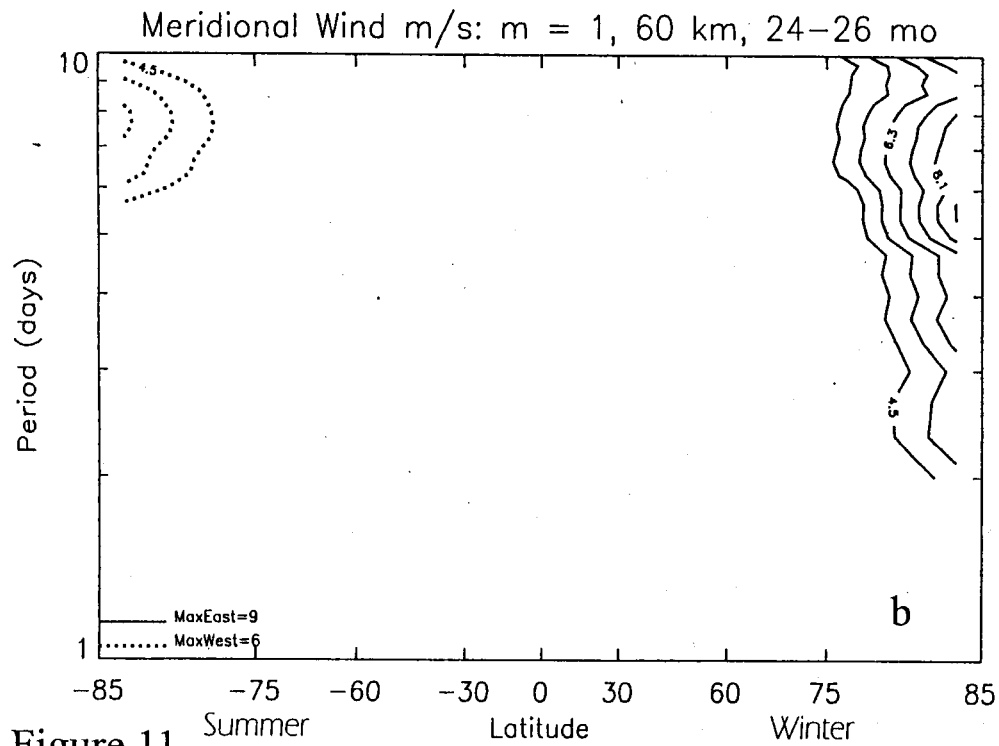
Meridional Wind m/s: m = 1, 60 km, 24–26 mo
Period (days)
10
1
MaxEast=9
MaxWest=6
b
−85 −75 −60 −30 0 30 60 75 85
Summer
Latitude
Winter
lim=3 cut=5 nwd=3 C812

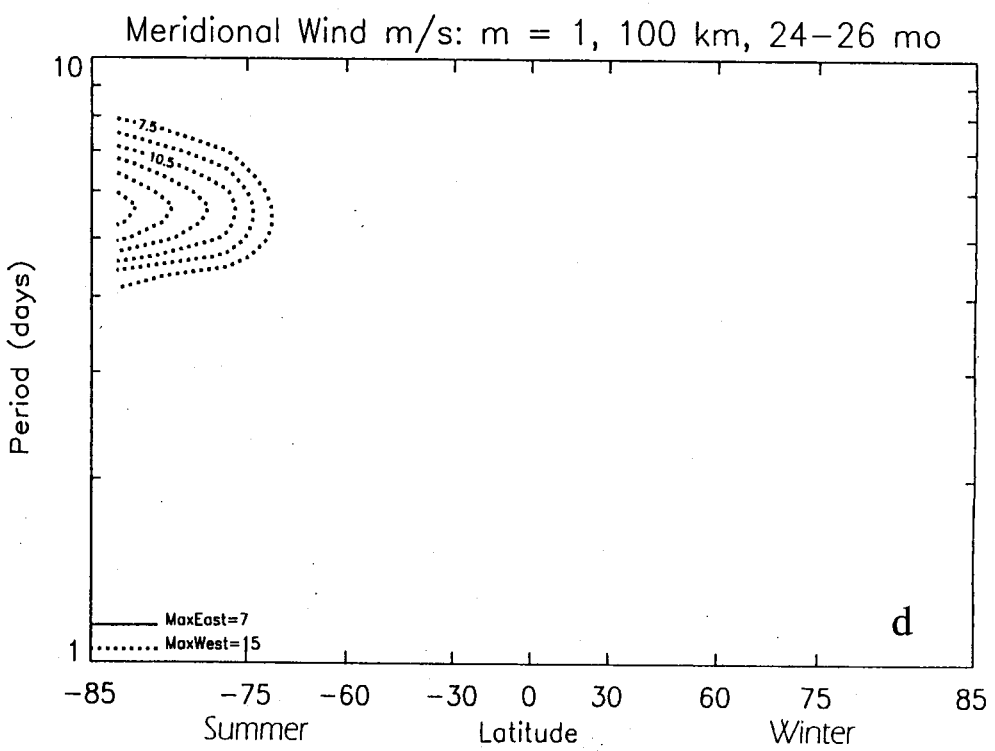
Meridional Wind m/s: m = 1, 100 km, 24–26 mo
Period (days)
10
1
MaxEast=7
MaxWest=15
d
−85 −75 −60 −30 0 30 60 75 85
Summer
Latitude
Winter
lim=3 cut=5 nwd=3 C808

Figure 11

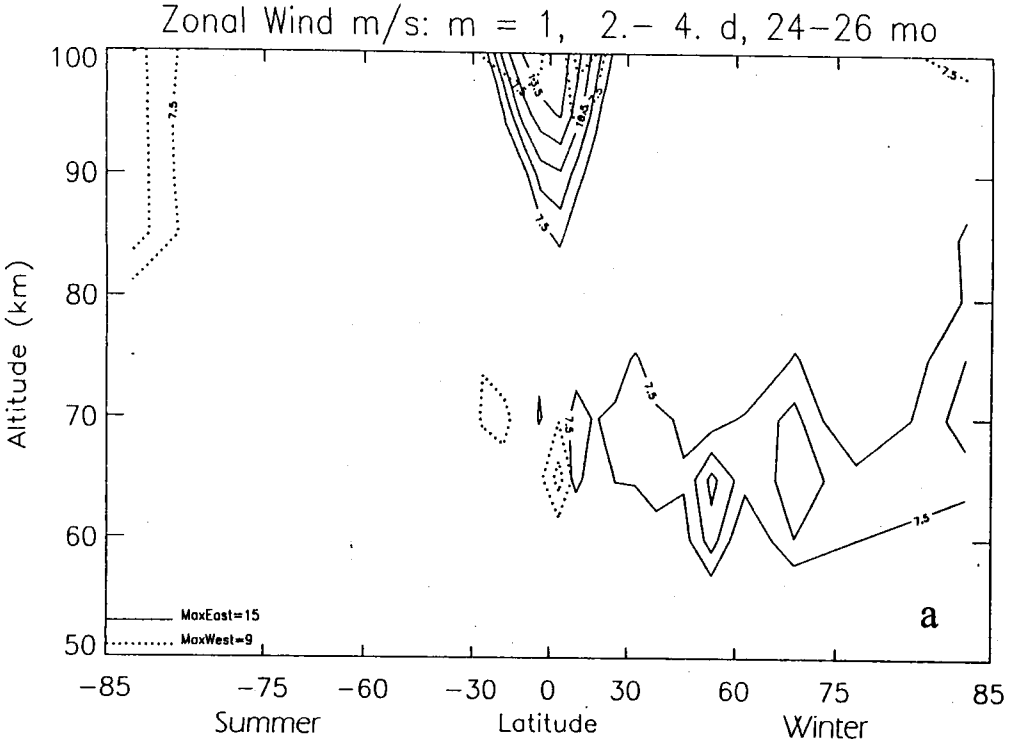

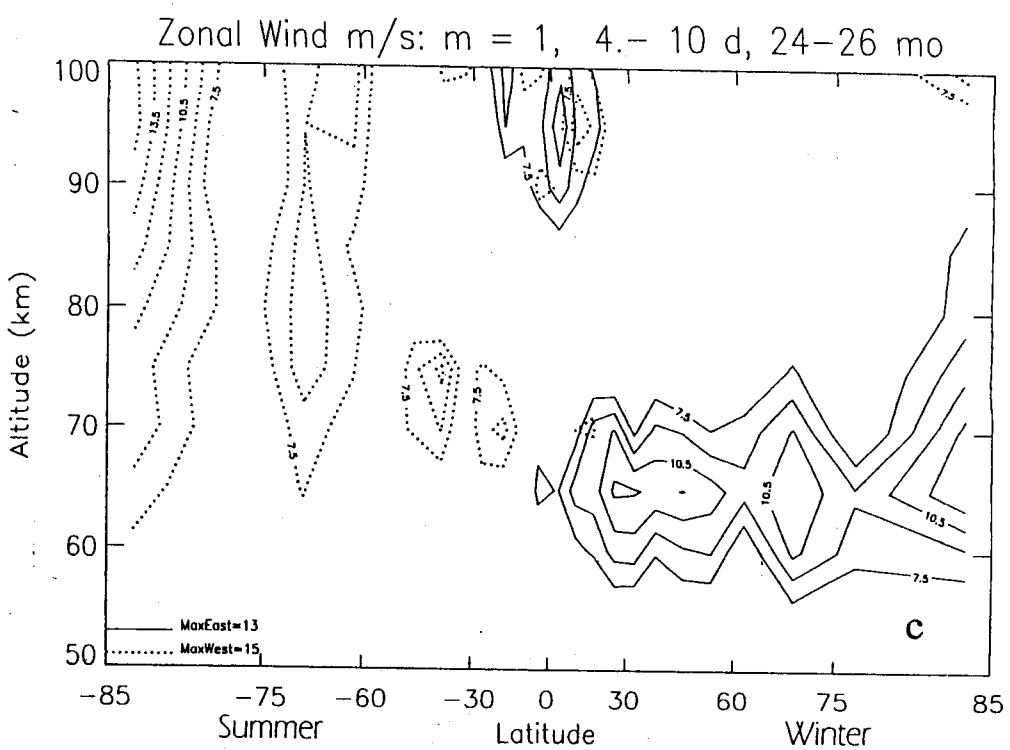

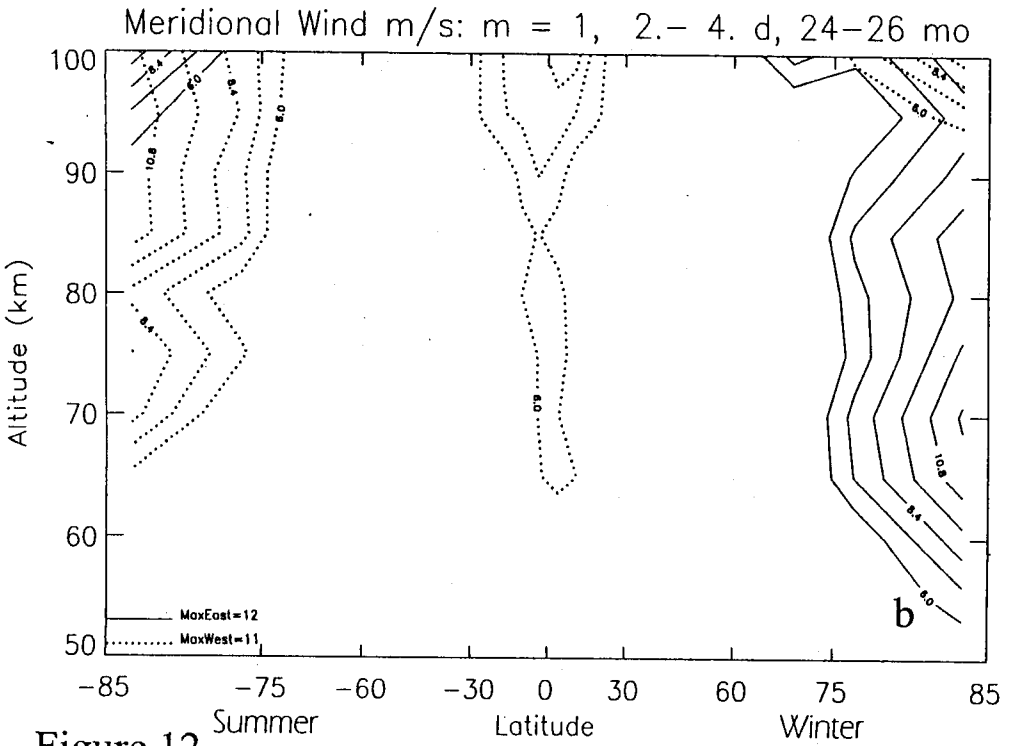

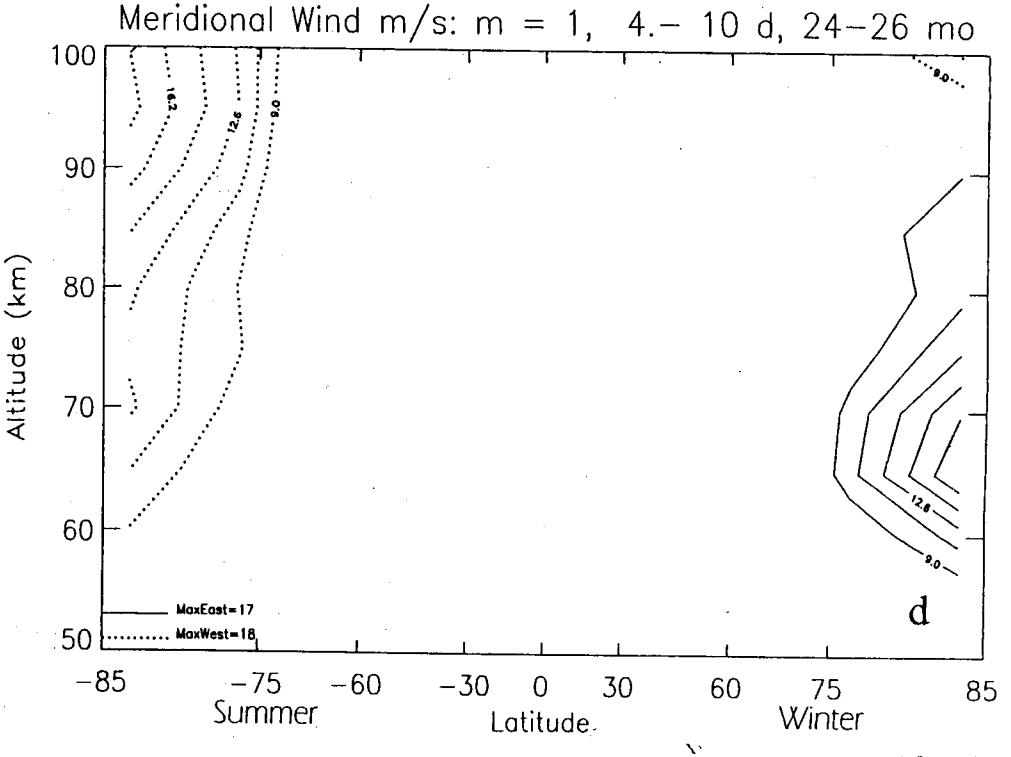

Figure 12

cut=5 nwd=2 C813

cut=5 nwd=2 C8